Compact Muon Solenoid

CMS is a world wide collaboration comprising 1543 physicists and engineers from 31 countries and 136 institutions

CMS is a general purpose proton-proton detector designed to run at the highest luminosity at the LHC It is also well adapted for studies at the initially lower luminosities. The main design goals of CMS are:

i) a highly performant **muon system**
ii) the best possible **electromagnetic calorimeter** consistent with (i)
iii) a high quality **central tracking** to achieve (i) and (ii)
iv) hermetic **hadron calorimeter**

Inner Tracker

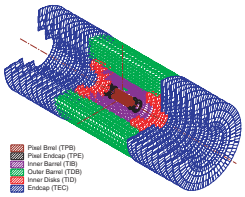

The tracking volume is given by a cylinder of a length of 6 m and a diameter of 2.6 m. Fine pitch Si detectors provide precise hits. Pixel detectors placed close to interaction region improve measurement of the track impact parameter and reconstruction of secondary vertices. In the central rapidity region (|η| <1.5) the momentum resolution is given by $\Delta p/p_t \approx 0.005 + 0.15\ p_t$ (p_t in TeV)

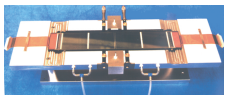

A Si module in its assembly jig. Strips from pairs of 6x6 cm Si detector are bonded together

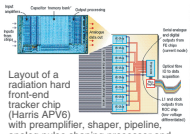

Layout of a radiation hard front-end tracker chip (Harris APV6) with preamplifier, shaper, pipeline, analog pulse shaping processor and multiplexer servicing 128 channels

Electromagnetic Calorimeter

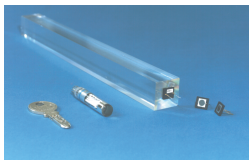

A full size (23cm long) lead tungstate crystal with a mounted APD

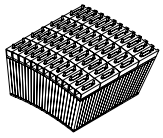

Lead tungstate crystals have a short radiation length (0.9cm) and Moliere radious (≈ 2cm). This yields a high performance compact calorimeter with fine segmentation. The scintillation light is detected by specially developed Silicon Avalanche Photodiodes (APD) which allow an amplification of up to ≈ 100

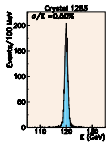

Energy resolution measured with 120 GeV electrons in a test beam. The distribution shown is for a sum of 3x3 crystals with lateral size of (2.2x2.2) cm²

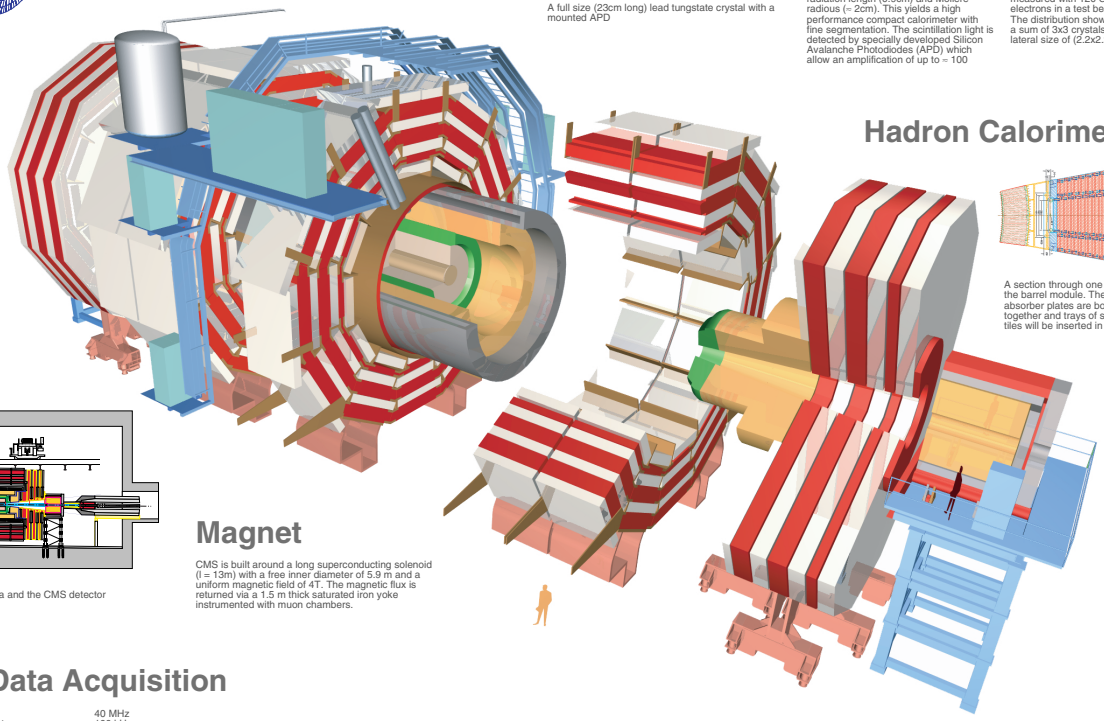

Hadron Calorimeter

A section through one sector of the barrel module. The copper absorber plates are bolted together and trays of scintillator tiles will be inserted in the gaps.

Installation

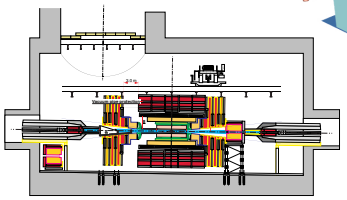

The underground experimental area and the CMS detector

Magnet

CMS is built around a long superconducting solenoid (l = 13m) with a free inner diameter of 5.9 m and a uniform magnetic field of 4T. The magnetic flux is returned via a 1.5 m thick saturated iron yoke instrumented with muon chambers.

Trigger and Data Acquisition

Collision rate	40 MHz
Level-1 Maximum trigger rate	100 kHz
Average event size	≈ 1 Mbyte
No. of In-Out units (200-5000 byte/event)	≈ 1000
Event builder (1000 port switch) bandwidth	1000 Gbit/s
Event filter computing power	≈ 5 10⁶ MIPS
Data production	≈ Tbyte/day

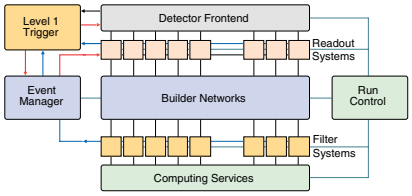

Muons

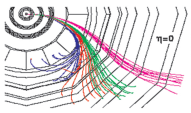

P_t = 3.5, 4.0, 4.5, 6.0 GeV

Centrally produced muons are measured 3 times: in the inner tracker, after the coil and in the return yoke. They are identified and measured in four identical muon stations using drift chambers in the barrel, cathode strip chambers in the endcaps and RPCs to assure redundancy in triggering

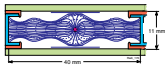

Drift Tube cross section (4x1 cm²)

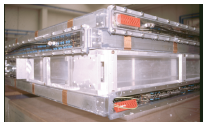

A full size prototype of the barrel drift chamber consisting of three groups of fourdetecting planes

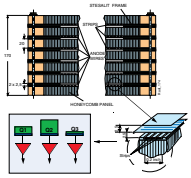

A six layer Cathode Strip Chamber. The detail of one layer is shown. Good resolution is obtained by using the centre of gravity of the charge induced on the strips

Physics Performance

H → γγ

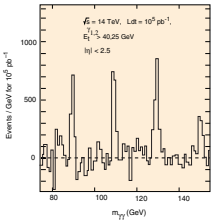

H →ZZ*→4e,2e 2μ,4μ

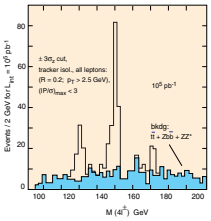

SUSY Higgs

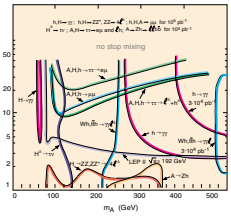

Sparticles

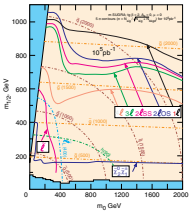

B-Physics

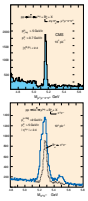

Heavy Ions

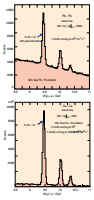

Mass Resolution

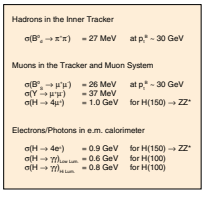

Large Hadron Collider

Calorimetry

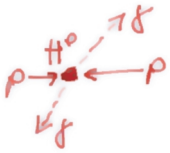

$p\,p \rightarrow H^0$
$\hookrightarrow \gamma\gamma$

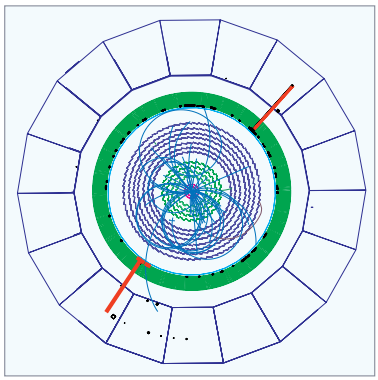

$p\,p \rightarrow H^0 \rightarrow Z\,Z$
$\hookrightarrow$ jet jet
$\hookrightarrow$ $e^+\,e^-$

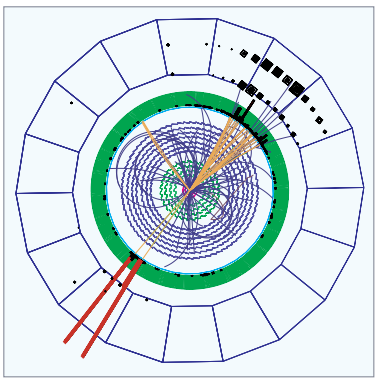

Electrons, photons and hadrons will be stopped by the calorimeters allowing their energy to be measured. The first calorimeter layer is designed to measure the energies of electrons and photons with high precision. Since these particles interact electromagnetically, it is called an electromagnetic calorimeter (ECAL). Particles which interact via the strong interaction, hadrons, deposit most of their energy in the next layer, the hadronic calorimeter (HCAL). Neutrinos escape direct detection but their presence can be inferred as an apparent energy imbalance in a collision

Electromagnetic Showers

The physics channel that imposes the strictest performance requirement for the electromagnetic calorimeter (ECAL) is the decay of the Higgs boson with mass in the range 100-140 GeV into two photons. All the terms making up the energy resolution (i.e. stochastic, constant and noise) have to be kept small and should be roughly equal at photon energies corresponding to approximately half the Higgs mass.

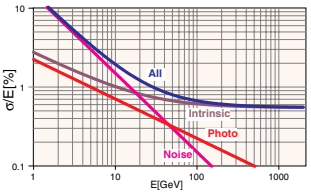

The resolution of the energy measurement of the electromagnetic calorimeter is driven by three major parameters:

- The shower containment and photostatictics
- The electronic noise and pileup energy
- The constant term

The full energy resolution is the sum of these terms and is shown in the figure on the left.

The resolution of the two-photon mass depends on the energy resolution and on the uncertainty on the angle between the two photons. If the vertex position is known, the angular error is negligible. However, if the only information available is the average spread of the interaction vertices, there is an additional 1.5 GeV contributing to the diphoton mass resolution.
At low luminosity the longitudinal position of the Higgs production vertex can be localized using high transverse momentum tracks found in the tracking system. Studies indicate that even at high luminosity the correct vertex can be located for a large fraction of the events using the same method.

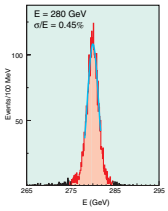

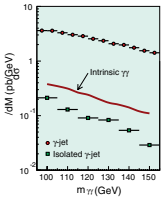

The ECAL must also have good two-shower separation capability to reject a sufficient number of π^0's carrying moderate transverse energy (20-40 GeV). The non-identification of these π^0's results in a very large background from photon+jet events, as shown on the left.
The last requirement on the ECAL is that of a large rapidity coverage. This is also true for the channel in which the Higgs boson decays to four charged leptons via one real and one virtual Z boson or via two real Z bosons.

The expected signal from the decay $H^0 \rightarrow \gamma\gamma$ for M_H=130 GeV, after 100 fb^{-1} collected at high luminosity.
On the left is the total diphoton mass spectrum, and on the right is the Higgs excess after background subtraction.

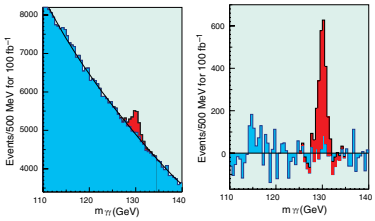

Hadronic Showers

The performance required from a hadron calorimeter (HCAL) is less constrained by the physics processes. The jet energy resolution is compromised by effects such as the jet-finding algorithm, the fragmentation process, the magnetic field and energy pile-up when running at high luminosity. The important characteristics are the transverse granularity and the η coverage.

The energy resolution in the Barrel HCAL for pions as a function of beam momentum is displayed for interactions in the HCAL only and in ECAL or HCAL. The absolute energy scale was set using 50 GeV pions interacting only in the HCAL.

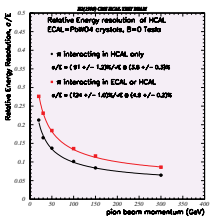

Measured energy resolution for electrons (upper figure) and pions (lower figure) for the HF calorimeter. In the hadronic energy study, the intrinsic resolution is found to scale with the logarithm of the energy (squares in the lower figure).

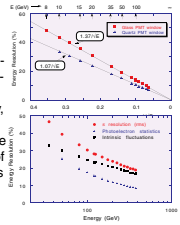

Emphasis is laid on hermeticity to ensure a good missing transverse energy measurement. Coverage up to |η|=5 is necessary for several reactions, e.g. a heavy Higgs decaying into two Z bosons which in turn give a lepton pair and jet pair. Adequate depth is also needed to contain high-energy jets and also to filter out the hadrons in jets for a cleaner muon measurement and trigger. A relatively fine transverse granularity is important in measuring the jet direction and also to separate two-jet combinations.

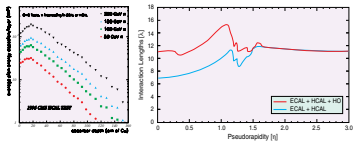

Left: shower profiles for pions of various momenta as a function of absorber depth in the calorimeter, as measured in beam tests. Right: depth of the calorimetry in absorption lengths. The full depth corresponds to approximately 11 absorption lengths of material.

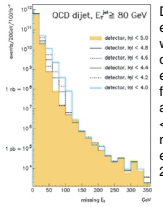

Distribution of missing energy associated with QCD dijets for different detector coverage; the figure justifies an HCAL coverage over the range |η| < 5, particularly for missing transverse energy in the range $25 < E_T < 125$ GeV.

The reconstruction of jets and dijet masses are keys to searches for high mass Higgs bosons. It is also very important in searching for Higgs bosons predicted by supersymmetry.

Possible signal from the production of a low mass supersymmetric Higgs boson (h) decaying into two b-jets. To identify this final state requires use of both the tracking detectors, to identify displaced vertices, and of the calorimetry, to measure and reconstruct the b-jet energies, over the full kinematic region.

$h \rightarrow b\bar{b}$ in mSUGRA

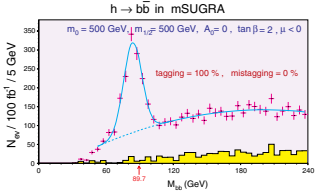

CMS collaboration

(144 Institutions with about 1700 scientists)

ARMENIA
- Yerevan Physics Inst., Yerevan

AUSTRIA
- HEPHY, Wien

BELARUS
- Institute of Nuclear Problems, Minsk
- National Centre of Part. and HEP, Minsk
- Res. Inst. of Applied Physical Probl., Minsk
- Byelorussian State Univ., Minsk

BELGIUM
- Univ. Instelling Antwerpen, Wilrijk
- Univ. Libre de Bruxelles, Brussels
- Vrije Universiteit Brussel, Brussels
- Univ. Catholique de Louvain, Louvain-la-Neuve
- Univ. de Mons-Hainaut, Mons

BULGARIA
- Inst. for Nucl. Res. and Nucl. Energy, Sofia
- Univ. of Sofia, Sofia

CHINA, PR
- Inst. of High Energy Physics, Beijing
- Peking Univ., Beijing
- Univ. for Science & Tech. of China, Hefei, Anhui

CROATIA
- Tech. Univ.of Split, Split
- Univ. of Split, Split

CYPRUS
- Univ. of Cyprus, Nicosia

ESTONIA
- Inst. of Chemical Phys. and Biophys., Tallinn

FINLAND
- Helsinki Institute of Physics, Helsinki
- Dpt.of Phys., Univ.of Helsinki, Helsinki
- Univ. of Jyväskylä, Jyväskylä
- Helsinki University of Technology, Helsinki
- Univ. of Oulu, Oulu
- Tampere Univ. of Tech., Tampere

FRANCE
- LAPP, IN2P3-CNRS, Annecy-le-Vieux
- IPN, IN2P3-CNRS, Univ. Lyon I, Villeurbanne
- LPNHE, Ecole Polytech., IN2P3-CNRS, Palaiseau
- DSM/DAPNIA, CEA/Saclay, Gif-sur-Yvette
- IRES, IN2P3-CNRS - ULP, UHA, LEPSI, Strasbourg

GEORGIA
- High Energy Phys. Inst., Tbilisi State Univ., Tbilisi
- Inst. of Physics Academy of Science, Tbilisi

GERMANY
- RWTH, I. Physik. Inst., Aachen
- RWTH, III. Physik. Inst. A, Aachen
- RWTH, III. Physik. Inst. B, Aachen
- Humboldt-Univ. zu Berlin, Berlin
- Inst. für Exp. Kernphysik, Karlsruhe

GREECE
- Univ. of Athens, Athens
- Inst. of Nucl. Phys. "Demokritos", Attiki
- Univ. of Ioánnina, Ioánnina

HUNGARY
- KFKI Res. Inst. for Part. & Nucl. Phys., Budapest
- Kossuth Lajos Univ., Debrecen
- Institute of Nuclear Research ATOMKI, Debrecen

INDIA
- Panjab Univ., Chandigarh
- Bhabha Atomic Res. Centre, Mumbai
- Univ. of Delhi South Campus, New Delhi
- TIFR - EHEP, Mumbai
- TIFR - HECR, Mumbai

ITALY
- Univ. di Bari e Sez. dell' INFN, Bari
- Univ. di Bologna e Sez. dell' INFN, Bologna
- Univ. di Catania e Sez. dell' INFN, Catania
- Univ. di Firenze e Sez. dell' INFN, Firenze
- Univ. di Genova e Sez. dell' INFN, Genova
- Univ. di Padova e Sez. dell' INFN, Padova
- Univ. di Pavia e Sez. dell' INFN, Pavia
- Univ. di Perugia e Sez. dell' INFN, Perugia
- Univ. di Pisa e Sez. dell' INFN, Pisa
- Univ. di Roma I e Sez. dell' INFN, Roma
- Univ. di Torino e Sez. dell'INFN, Torino

KOREA
- Cheju National University, Cheju
- Chonnam National University, Kwangju
- Choongbuk National University, Chongju
- Dongshin University, Naju
- Kangnung National University, Kangnung
- Kangwon National University, Chunchon
- Kon-Kuk University, Seoul
- Korea University, Seoul
- Kyungpook National University, Taegu
- Pohang University of Science and Technology, Pohang
- Gyeongsang National University, Jinju
- Seonam University, Namwon
- Seoul National Univ. of Education, Seoul
- Wonkwang University, Iri

PAKISTAN
- Quaid-I-Azam Univ., Islamabad
- Ghulam Ishaq Khan Institute, Swabi

POLAND
- Inst. of Exp. Phys., Warsaw
- Soltan Inst. for Nucl. Studies, Warsaw

PORTUGAL
- LIP, Lisboa

RUSSIA
- JINR, Dubna
- Inst. for Nucl. Res., Moscow
- Inst. for Theoretical and Exp. Phys., Moscow
- P.N. Lebedev Phys. Inst., Moscow
- Moscow State Univ., Moscow
- Budker Inst. for Nucl. Phys., Novosibirsk
- Inst. for High Energy Phys., Protvino
- Petersburg Nucl. Phys. Inst., Gatchina (St Petersburg)

SLOVAK REPUBLIC
- Slovak University of Technology, Bratislava

SPAIN
- CIEMAT, Madrid
- Univ. Autónoma de Madrid, Madrid
- Univ. de Oviedo, Oviedo
- IFCA, CSIC-Univ. de Cantabria, Santander

SWITZERLAND
- Univ. Basel, Basel
- CERN, Geneva
- Paul Scherrer Inst., Villigen
- Inst. für Teilchenphysik, ETH, Zurich
- Univ. Zürich, Zurich

TURKEY
- Cukurova Univ., Adana
- Middle East Technical Univ., Ankara

UKRAINE
- Inst. of Single Crystals of Nat. Acad. of Science, Kharkov
- Kharkov Inst. of Phys. and Tech., Kharkov
- Kharkov State Univ., Kharkov

UNITED KINGDOM
- Univ. of Bristol, Bristol
- Brunel Univ., Uxbridge
- Imperial College, Univ. of London, London
- RAL, Didcot

USA
- Univ. of Alabama, Tuscaloosa
- Iowa State Univ., Ames
- Boston Univ., Boston
- California Inst. of Tech., Pasadena
- Carnegie Mellon Univ., Pittsburgh
- Univ. of Illinois at Chicago, Chicago
- Fairfield Univ., Fairfield
- Fermi National Accelerator Lab., Batavia
- Florida State Univ. - HEPG, Tallahassee
- Florida State Univ. - SCRI, Tallahassee
- Univ. of Florida, Gainesville
- The Univ. of Iowa, Iowa City
- Johns Hopkins Univ., Baltimore
- LLNL, Livermore
- Los Alamos Nat. Lab., Los Alamos
- Univ. of Maryland, College Park
- Univ. of Minnesota, Minneapolis
- Univ. of Mississippi, Oxford
- Massachusetts Inst. of Tech., Cambridge
- Univ. of Nebraska-Lincoln, Lincoln
- Northeastern Univ., Boston
- Northwestern Univ., Evanston
- Univ. of Notre Dame, Notre Dame
- The Ohio State Univ., Columbus
- Princeton Univ., Princeton
- Purdue Univ., West Lafayette
- Rice Univ., Houston
- Univ. of California, Riverside
- Univ. of Rochester, Rochester
- Rutgers, the State Univ. of New Jersey, Piscataway
- Texas Tech Univ., Lubbock
- Univ. of Texas at Dallas, Richardson
- Univ. of California at Davis, Davis
- UCLA, Los Angeles
- Univ. of California San Diego, La Jolla
- Virginia Polytech. Inst. and State Univ., Blacksburg
- Univ. of Wisconsin, Madison

UZBEKISTAN
- Inst. of Nucl. Phys. of the Uzbekistan Acad. of Sciences, Tashkent

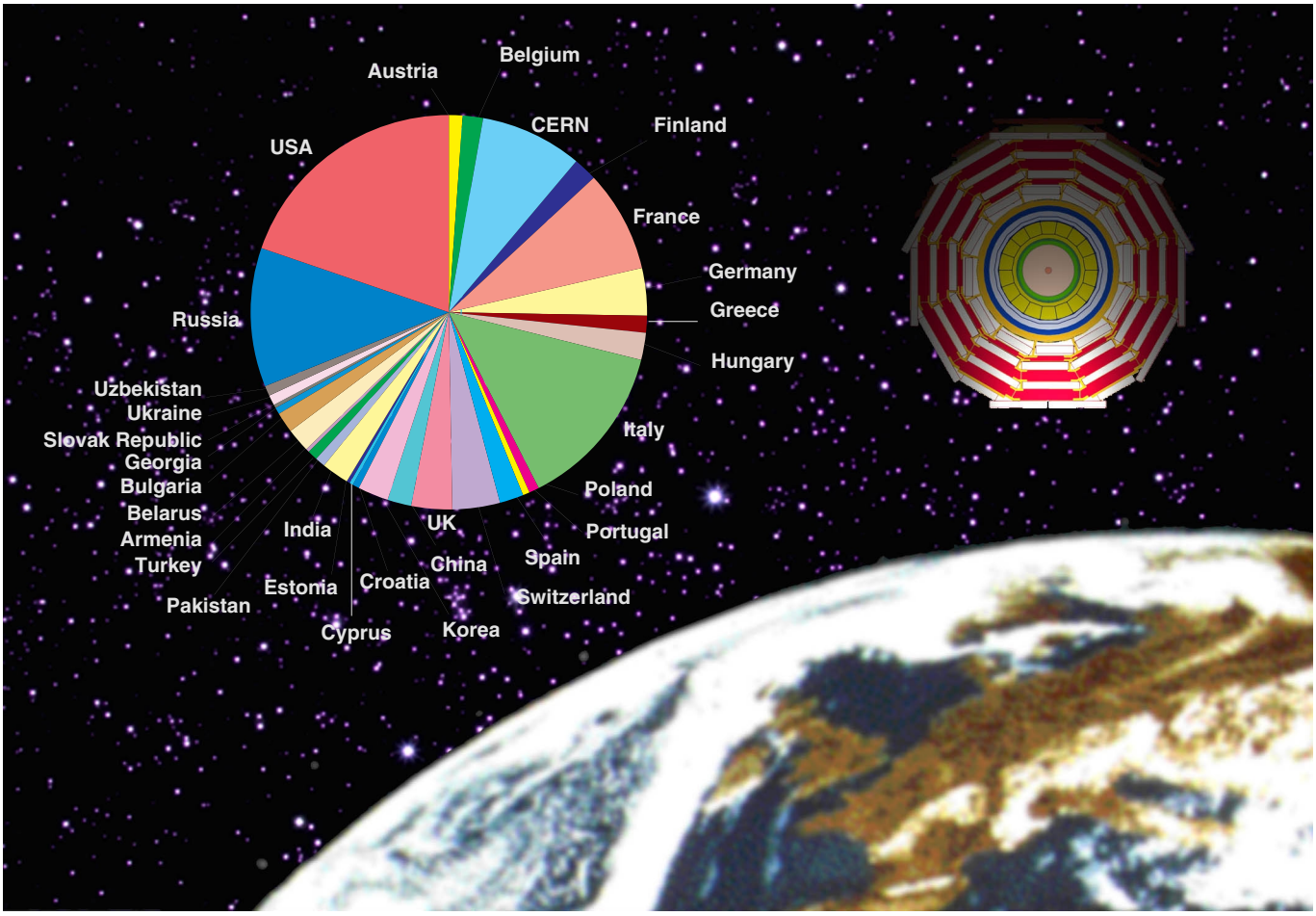

23.07.98

Electromagnetic calorimeter

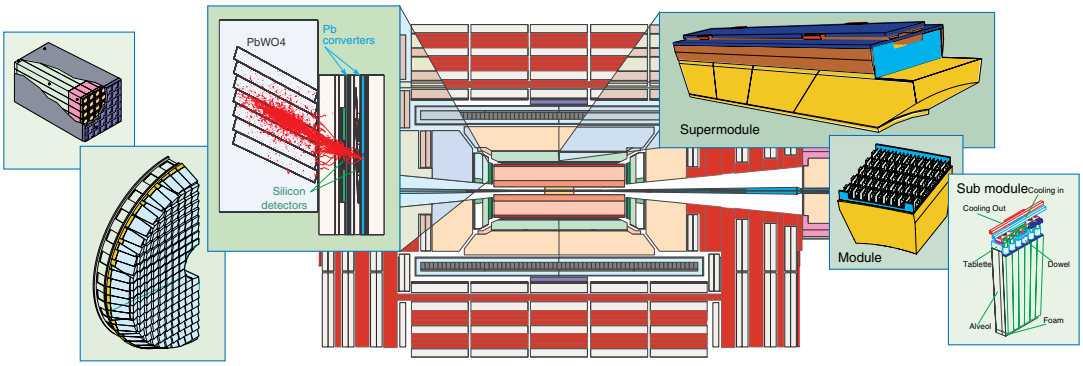

One of the principal CMS design objectives is to construct a very high performance electromagnetic calorimeter. A scintillating crystal calorimeter offers excellent performance for energy resolution since almost all of the energy of electrons and photons is deposited within the crystal volume. CMS has chosen lead tungstate crystals which have high density, a small Molière radius and a short radiation length allowing for a very compact calorimeter system. A high-resolution crystal calorimeter enhances the H→γγ discovery potential at the initially lower luminosities at the LHC

Lead-Tungstate Crystals

The CMS electromagnetic calorimeter will consist of over 80,000 lead-tungstate ($PbWO_4$) crystals equipped with avalanche photodiodes or vacuum phototriodes and associated electronics operating in a challenging environment: a magnetic field of 4T, a time of 25 ns between bunch crossings, a radiation dose of ≈ 1-2 kGy/year for LHC operation at maximum luminosity, and also difficult access for maintenance

After an intensive R&D program, lead tungstate crystals were chosen because they offer the best prospects of meeting these demanding requirements. The choice was based on the following considerations:

- $PbWO_4$ has a short radiation length and a small Molière radius
- it is a fast scintillator
- it is relatively easy to produce from readily available raw materials and substantial experience and production capacity already exist in China and Russia

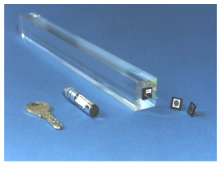

The crystals have a front face of about 22x22 mm^2 — which matches well the Molière radius of 22 mm. To limit fluctuations on the longitudinal shower leakage of high-energy electrons and photons, the crystals must have a total thickness of 26 radiation lengths — corresponding to a crystal length of only 23 cm

$PbWO_4$ is intrinsically radiation-hard, but non-optimized crystals do suffer from radiation damage. The R&D program of the last few years has led to a better understanding of the damage mechanism. The main conclusion is that radiation affects neither the scintillation mechanism nor the uniformity of the light yield along the crystal. It only affects the transparency of the crystals through the formation of color centers and the transport of light is changed by self-absorption of the crystals. This light loss can be monitored by a light-injection system

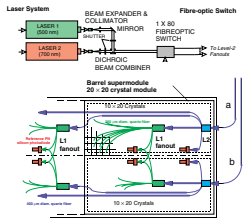

The light monitoring system, shown on the left, is designed to inject light pulses into each crystal to measure the optical transmission. The pulses are distributed via an optical-fibre system. The system is designed to continuously monitor the calorimete

Preshower Detector

CMS will utilize a preshower detector in the endcap region (rapidity range $1.65 < |\eta| < 2.6$). Its main function is to provide γ–π^0 separation

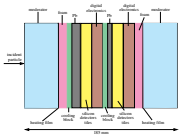

The preshower detector contains two thin lead converters followed by silicon strip detector planes placed in front of the ECAL.

The measurement of the energy deposition in the ~2 mm pitch silicon strips allows the determination of the impact position of the electromagnetic shower by a charge-weighted-average algorithm with very good accuracy (~300μm at 50 GeV). The fine granularity of the detector enables the separation of single showers from overlaps of two close showers due to the photons from π^0 decays

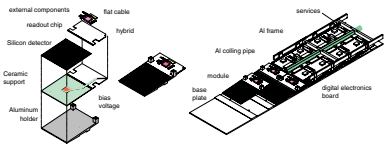

The active planes of silicon detectors are built from a large number of identical modules each of which contains an individual detector, as shown above. A module contains an aluminum tile ('holder') onto which a ceramic support is glued. A silicon detector, subdivided into 32 strips at 1.9 mm pitch, is then glued and bonded to the ceramic. The hybrid containing the analog front-end electronics is also glued and bonded to the ceramic. The modules are then assembled on long ladders which contain two columns of adjacent detectors

The π^0 rejection algorithm using the preshower compares the highest signal (summed in 1, 2 or 3 adjacent strips) with the total signal in 21 adjacent strips centered on the highest-signal strip. The fraction of the two energies, F, is then used to select photons (and reject π^0's)

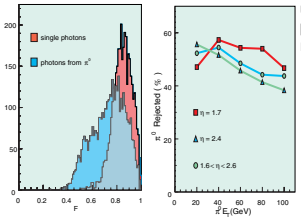

The rejection obtained with this simple algorithm approaches a factor of 3 and is fairly independent of E_T.

Readout

The scintillation light from the crystals must be captured by a photodetector, amplified and digitized. A schematic of the readout sequence is shown in the figure below

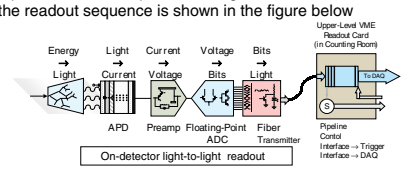

The first element is the $PbWO_4$ crystal which converts energy into light. The light is converted into a photocurrent by the photodetector. The relatively low light yield of the crystal necessitates a preamplifier in order to convert the photocurrent into a voltage waveform. The signal is then acquired and digitized. The resulting data are transported off the detector via optical fibre to the upper-level readout

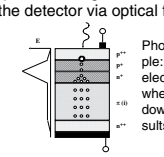

Photodetector (Avalanche Photodiode) principle: Photons convert in the p^{++} layer. Photoelectrons drift towards the abrupt p-n junction where ionization starts and avalanche breakdown occurs. The avalanche breakdown results in impact electron multiplication.

To avoid the design and construction of a very large quantity of radiation-hard electronics, the data are transported, immediately after the digitization step, to the counting room by fibreoptic links

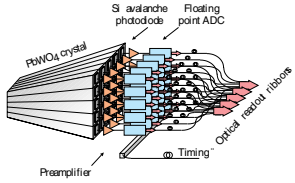

The upper level readout has four main functions:

- formation of trigger tower energy sums
- pipelining (storing the data until receipt of a Level-1 trigger decision)
- transmission of the data from the triggered event to the Data Acquisition System
- providing interface functions for the on-detector electronics

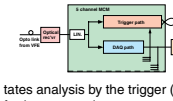

Layout of the upper-level readout. The optical receiver deserializes the data from the Very Front-Ends. The linearizer transforms the incoming data to a representation which facilitates analysis by the trigger (e.g. formation of energy sums) without further conversions

Hadronic calorimeter

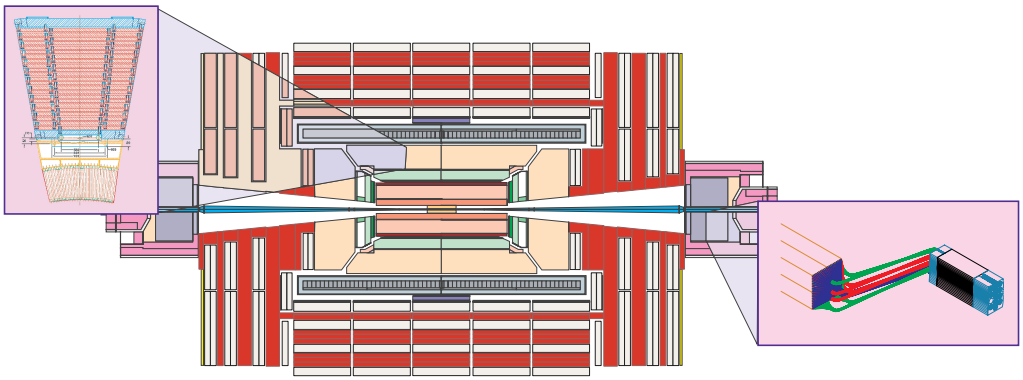

The Hadronic Calorimeter (HCAL), plays an essential role in the identification and measurement of quarks, gluons, and neutrinos by measuring the energy and direction of jets and of missing transverse energy flow in events. Missing energy forms a crucial signature of new particles, like the supersymmetric partners of quarks and gluons. For good missing energy resolution, a hermetic calorimetry coverage to $|\eta|=5$ is required. The HCAL will also aid in the identification of electrons, photons and muons in conjunction with the tracker, electromagnetic calorimeter, and muon systems

Barrel & Endcap

The hadron barrel (HB) and hadron endcap (HE) calorimetesr are sampling calorimeters with 50 mm thick copper absorber plates which are interleaved with 4 mm thick scintillator sheets.

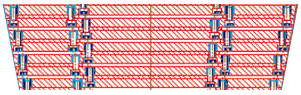

Copper has been selected as the absorber material because of its density. The HB is constructed of two half-barrels each of 4.3 meter length. The HE consists of two large structures, situated at each end of the barrel detector and within the region of high magnetic field. Because the barrel HCAL inside the coil is not sufficiently thick to contain all the energy of high energy showers, additional scintillation layers (HOB) are placed just outside the magnet coil. The full depth of the combined HB and HOB detectors is approximately 11 absorption lengths.

Light emission from the tiles is in the blue-violet, with wavelength in the range λ = 410-425 nm. This light is absorbed by the wave-shifting fibers which fluoresce in the green at λ = 490 nm. The green, waveshifted light is conveyed via clear fiber waveguides to connectors at the ends of the megatiles.

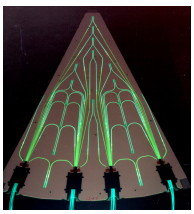

Megatiles are large sheets of plastic scintillator which are subdivided into component scintillator tiles, of size $\Delta\eta \times \Delta\phi$ = 0.87 x 0.87 to provide for reconstruction of hadronic showers. Scintillation signals from the megatiles are detected using waveshifting fibers. The fiber diameter is just under 1 mm.

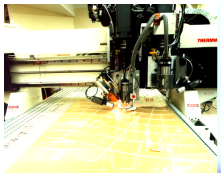

Megatiles are cut out on a special milling machine called a Thermwood. The Thermwood is programmed to cut tiles of varying dimension and also to machine keyhole grooves in the plastic into which the waveshifting fibers are inserted. The gaps between adjacent tiles are filled with diffuse reflective paint to provide optical isolation.

Forward

There are two hadronic forward (HF) calorimeters, one located at each end of the CMS detector, which complete the HCAL coverage to $|\eta| = 5$. The HF detectors are situated in a harsh radiation field and cannot be constructed of conventional scintillator and waveshifter materials. Instead, the HF is built of steel absorber plates; steel suffers less activation under irradiation than copper. Hadronic showers are sampled at various depths by radiation-resistant quartz fibers, of selected lengths, which are inserted into the absorber plates.

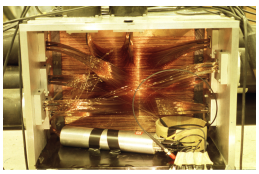

Quartz fibers of 300 µm diameter are shown threaded into an early prototype HF test module which utilized copper absorber. This view is looking directly into the beam.

The energy of jets is measured from the Cerenkov light signals produced as charged particles pass through the quartz fibers. These signals result principally from the electromagnetic component of showers, which results in excellent directional information for jet reconstruction. Fiber optics convey the Cerenkov signals to photomultiplier tubes which are located in radiation shielded zones to the side and behind each calorimeter.

Spectral analysis of data taken during intense radiation exposure of an HF prototype, underway at LIL. Quartz fibers with various claddings were tested.

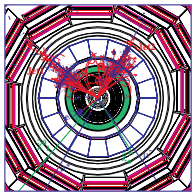

Supersymmetric particles may reveal themselves in some spectacular events involving leptons, jets and missing energy.
In this simulated event, jets are observed in the HB calorimeter. The hermeticity of the HCAL (the HB, HE and HF detectors working together) is used to identify the substantial missing energy in the event.

Readout

Light from waveshifting fibers is "piped" via clear optical waveguide fibers to readout boxes located at the ends of the barrel and endcap detectors at large radii relative to the beam, yet within the region of high magnetic field. For HCAL detector elements in the barrel region located beyond the magnet coil, the readout boxes are positioned on the iron flux return outside the muon system.

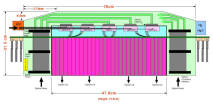

Within the readout boxes, the optical signals from the megatile layers are grouped into "towers" according to $\Delta\eta \times \Delta\varphi$ interval. These tower signals are detected and converted into fast electronic signals by photosensors.

For the barrel and endcap detectors, the photosensors are hybrid photodiodes (HPDs). For the forward detectors, conventional photomultiplier tubes are used.

The HPDs are new devices consisting of a fiber-optic entrance window onto which a multi-alkali photocathode is deposited, followed by a gap of several millimeters over which a large applied electric field accelerates photoelectrons onto a silicon diode target. The target is subdivided into individual readout elements called pixels. For CMS, 19-channel and 73-channel HPDs will be used.

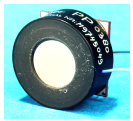

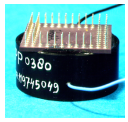

The gain of HPDs is typically 2000-3000 for applied voltages of 10-15 kV. HPDs are capable of operating in high axial magnetic fields and provide a linear response over a large dynamic range from minimum ionizing particles (muons) up to 3 TeV hadron showers. The electronic signals from the HPDs are processed and digitized using special front end integrated circuits called QIE chips. QIE is an acronym for charge (Q) integration (I) and encode (E).

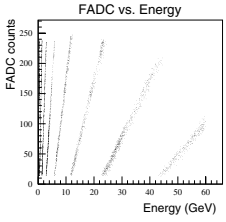

The demand of large dynamic range in the energy measurement is accomplished through a multi-range technique. The encoded output signals are then sent via fiber-optic links to the trigger and data acquisition systems.

Heavy Ions

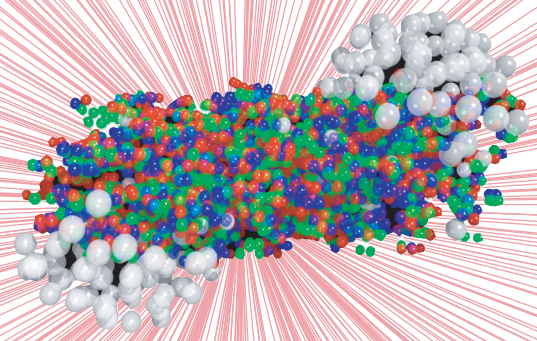

The LHC will not only collide proton beams: some periods of time will be spent colliding beams of nuclei, such as calcium (Ca) and lead (Pb). Collisions between these nuclei will produce “little bangs” at a temperature of ~ 200 MeV (around 100,000 times that of the centre of the sun), and an energy density up to 30 GeV/fm^3 (200 times that of normal nuclear matter). Under these extreme conditions, which mimic those of the very early Universe ~ 10 μs after the Big Bang, the constituent protons, neutrons and gluons (the carriers of the inter-quark force) “melt” to form a “quark-gluon plasma (QGP)”. CMS is very well suited to study some aspects of the formation of the QGP through the detection of muons and jets

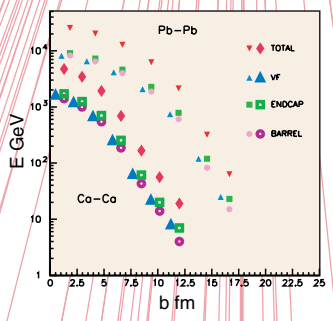

We can differentiate peripheral events, which have no plasma formation, from central events, where the QGP is expected, by measuring the impact parameter of the collision. The impact parameter of the nucleus-nucleus collision will be given by the transverse energy flow measured in CMS calorimetry (electromagnetic and hadronic) over a wide rapidity range, up to |η|=5

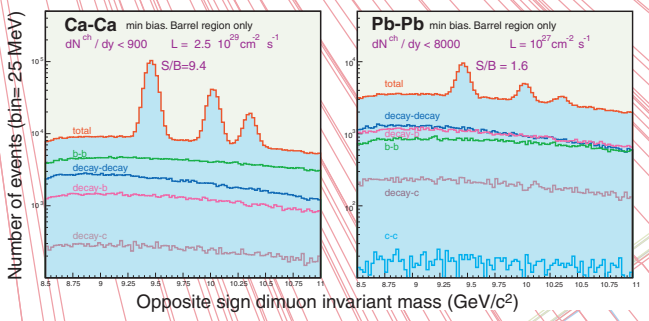

One of the best signatures proposed as evidence for quark-gluon plasma formation is the suppression of heavy quark vector mesons due to colour screening. CMS is particularly well suited to study this suppresion within the Υ family and to a lesser extent for the J/ψ and ψ' through their dimuon decay channel.The main background comes from the uncorrelated π/K decays and b production.The spectra are estimated for 1 month (1.2×10^{6}s), without suppression, and for muons reconstructed in the |η|<1.3 region where a reconstruction algorithm based on a (δφ, P_T) roads technique has been developed. A reconstruction efficiency plateau at 92% extends up to dN$^{\pm}$ /dη=2000 and decreases to 64% for dN$^{\pm}$/dη=8000. The resolution at the Υ mass (the peak at 9.46 GeV) is 50 MeV.

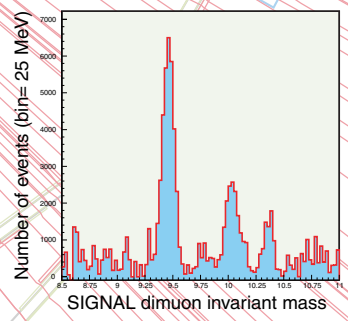

Opposite sign dimuon invariant mass spectrum for Pb-Pb events after subtracting the uncorrelated background from like-sign dimuon events

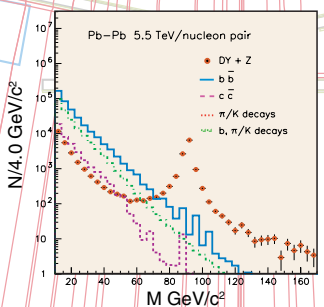

Detection of the $Z \rightarrow \mu^+\mu^-$ will provide a good reference point as the point-like Z-boson is not expected to be affected by the plasma. The different sources of background are shown for muons with P_T>5 GeV/c detected in the CMS barrel region

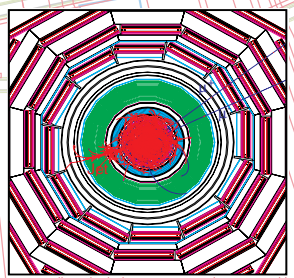

Z+jet event in the Heavy Ion collision

Z ($\rightarrow \mu^+\mu^-$)+ jet event with P_T^Z=100 GeV in a Pb-Pb collision in CMS. Charged particles with a multiplicity density dN^{ch}/dy=5000 are drawn in the slice Δη=0.1 around one of muons from the Z decay. Such events could be used to investigate jet quenching as P_T^Z is known from $Z \rightarrow \mu^+\mu^-$. For a one month run (1.2×10^{6}s) we expect 600 Z ($\rightarrow \mu^+\mu^-$) +jet events with E_T^{jet}>50 GeV in |η|<1.5

Hard jet production is another possible probe to study the formation of the QGP. Energy loss of the gluon (quark) in traversing dense matter leads to “quenching”, i.e. the suppression of high P_T jets. Di-jet quenching, the enhancement of the monojet/dijet ratio and the study of jets in Z+jet and γ+jet channels are possible probes. Modified WINDOW and cone type algorithms have been developed for extraction of high-P_T jets from the heavy ion background. The highest-E_T jet yield and the possibility to diminish the number of false jets depend on the chosen radius (R). The best performance is obtained for R=0.3 - 0.5

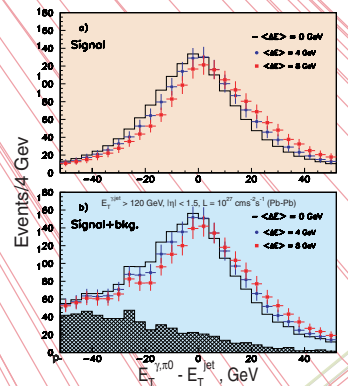

The $E_T^{\gamma/\pi 0}$-E_T^{jet} distribution for different jet energy losses is estimated for one month run (1.2x10^6 s) for barrel calorimeters (|η|<1.5). The main background sources are jet+jet events where one of the jets has a leading π^0

Higgs physics

The Standard Model (SM) of Particle Physics has unified the Electromagnetic interaction (carrier: γ) and the weak interaction (carriers: W^+, W^-, Z^0). Yet these four bosons are very different: the γ is massless whereas the $W^\pm$ and Z^0 are quite massive (80 – 90 GeV). In the framework of the SM particles acquire mass through their interaction with the Higgs field. This implies the existence of a new particle: the Higgs boson H^0. The theory does not predict the mass of the H^0, but it does predict its production rate and decay modes for each possible mass. CMS has been optimized to discover the Higgs in the full expected mass range $0.08\ \text{TeV} \lesssim M_H \lesssim 1\ \text{TeV}$

The decay signature of the Higgs depends on its mass:

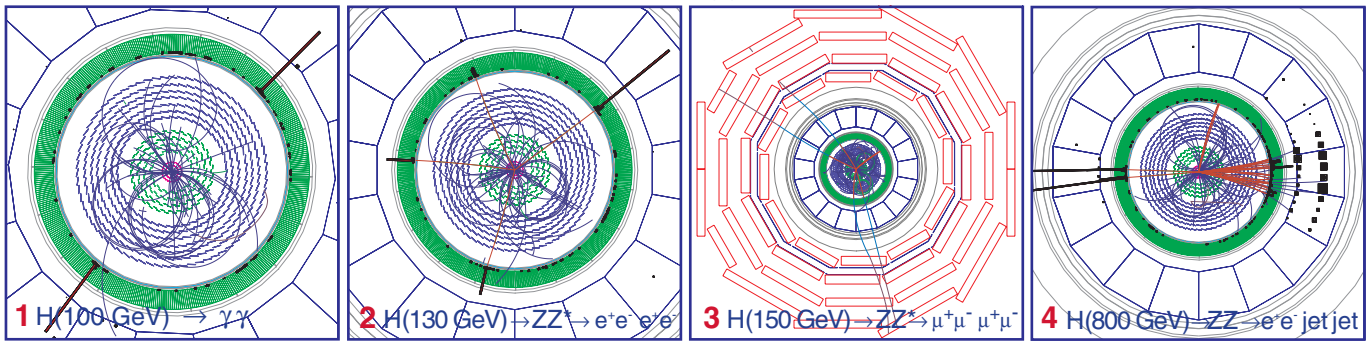

1. $H^0 \to \gamma\gamma$ is the most promising channel if M_H is in the range 80 – 140 GeV. The high performance $PbWO_4$ crystal electromagnetic calorimeter in CMS has been optimized for this search. The $\gamma\gamma$ mass resolution at $M\gamma\gamma \sim 100$ GeV is better than 1%, resulting in a S/B of ≈1/20. With larger data samples ($\geq 10^5$ pb^{-1}) the "associated" modes ($pp \to WH^0$ and $pp \to t\bar{t}H^0$) should give higher S/B ratios for the same H^0 decay channel

2-3. In the M_H range 130 - 700 GeV the most promising channel is $H^0 \to ZZ^* \to 2\ell^+2\ell^-$ or $H^0 \to ZZ \to 2\ell^+2\ell^-$. The detection relies on the excellent performance from the muon chambers, the tracker and the electromagnetic calorimeter.
For $M_H \leq 170$ GeV a mass resolution of ~1 GeV should be achieved with the 4 Tesla magnetic field and the high resolution of the crystal calorimeter

4. For the highest M_H, in the range 0.5 - 1 TeV, the promising channels for 10^5 pb^{-1} are $H^0 \to ZZ \to \ell^+\ell^-\nu\nu$, $H^0 \to ZZ \to \ell^+\ell^-$ jj and $H^0 \to W^+W^- \to \ell^\pm\nu$jj.
Detection relies on leptons, jets and missing transverse energy (E_t^{miss}), for which the hadronic calorimeter(HCAL) performance is very important

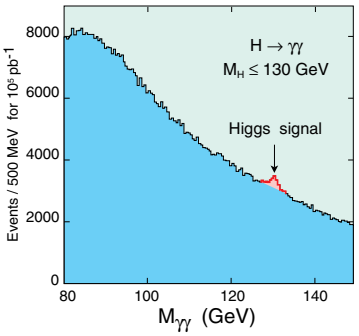

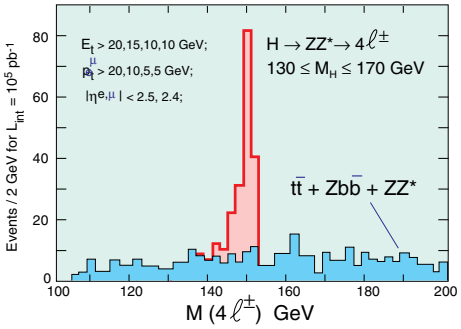

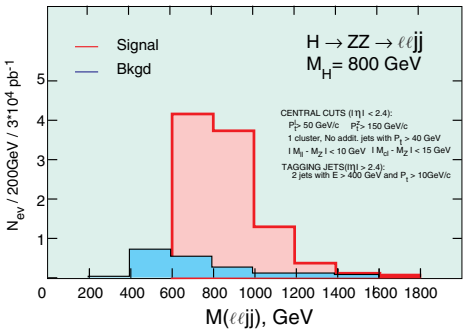

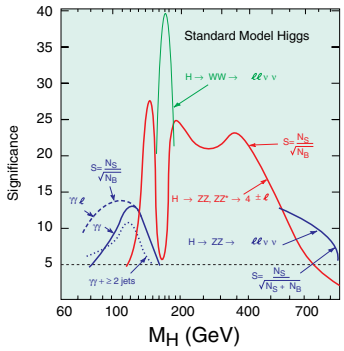

Observability of the SM Higgs in CMS with 10^5 pb^{-1}. The CMS detector can probe the entire mass range up to $M_H \sim 1$ TeV with a signal significance well above 5σ

Some extensions of the Standard Model involve a richer set of Higgs bosons: in the Minimal Supersymmetric SM there are five new bosons (h^0, H^0, A^0, H^+, H^-). Their discovery involves the use of more complicated signatures, such as the identification of a jet as coming from b quarks

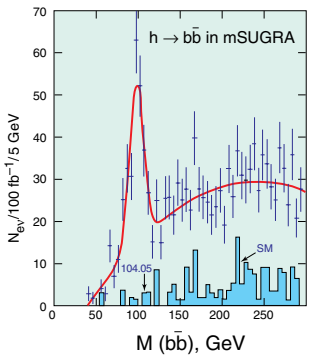

Installation

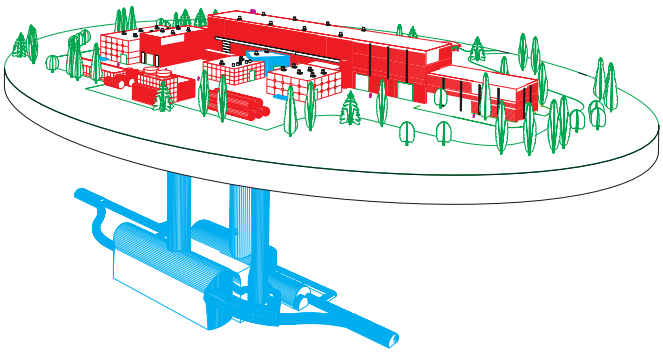

CMS experimental area overview

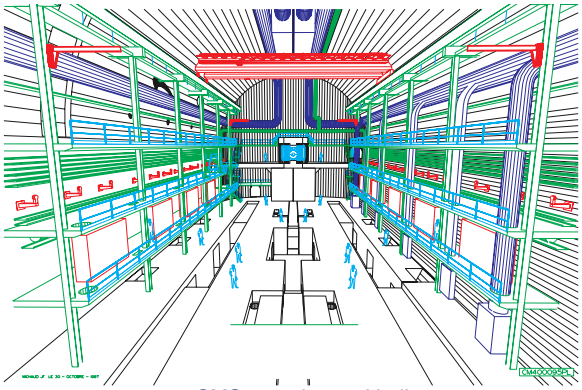

CMS experimental hall

The plan for the construction and installation of the CMS detector in the experimental hall minimizes any interference with the exploitation of LEP to reduce time and costs. To achieve this, the assembly and testing of the magnet will take place in a large surface hall before lowering it into the underground experimental cavern. This solution allows CMS to start by the end of 1999 while LEP is still in operation. The choice of using a surface hall rather than the underground area, allows the construction of the magnet and detectors in parallel with the civil engineering works. CMS will be located at Cessy (LHC point 5)

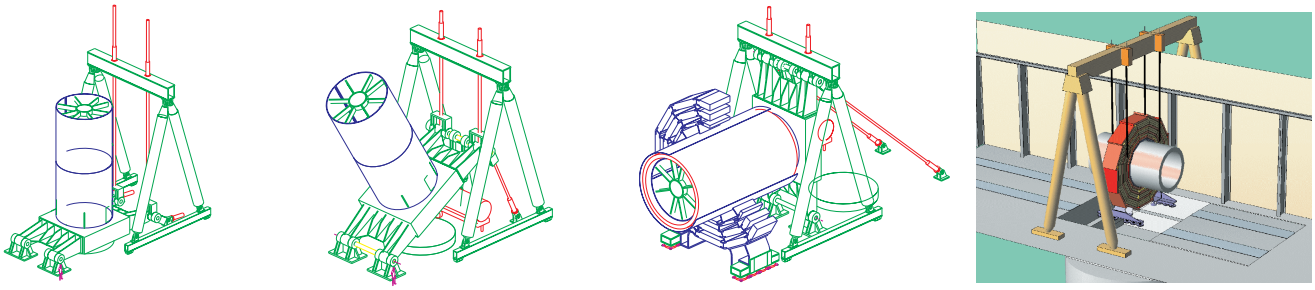

Rotation of the winded coil to horizontal position, sliding in the central yoke and lifting in the pit

The surface building complex will be located at Cessy (point 5). During the construction phase the main assembly hall will have a length of 140 m, a width and height of 23.5 m. After the magnet has been tested, these dimensions will be reduced to a length of about 100 m and a height of 16 m, thus having no major impact on the environment. The surface assembly hall will also have two temporary alcoves which will be used as a garage for the HB when moving large sections of the experiment through the hall. A third alcove will be used for testing the external cryogenics and the power supply before the surface test.

A temporary addition to the assembly hall, SXL5, is built to allow the final on-site reinforcement of the coil superconductor. Other buildings to be used for gas, primary cryogenics, ventilation, etc. will be also built on the surface at point 5.

The underground areas include the experimental cavern UXC5, the auxiliary cavern USC5, the access pits, PX56 and PM54, and the LHC machine by-pass. They are separated from the surface hall by a mobile radiation shielding plug situated at the top of PX56. The magnet is used as the principal structural element to support all barrel detector components.

The central barrel ring of the yoke support the superconducting coil through the vacuum tank. The other four barrel rings and end cap disks slide on common rails, running in the beam direction, to allow insertion and maintenance of the muon stations.

CMS experimental rotation of the winded coil to horizontal position, sliding in the central yoke and lifting in the pit.

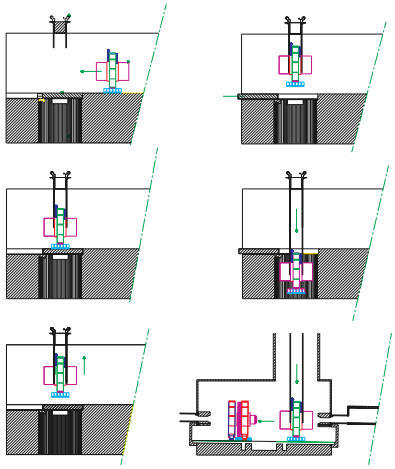

All the barrel sub-detectors, calorimeters (HB, EB) and tracker, are supported by the inner shell of the vacuum tank via a system of rails welded to it in the horizontal plane. The end cap detectors (ME, HE, EE) are supported by the end cap yokes. At each end of the inner tracker, a 1 m long cylindrical section of beam pipe is provided for in-situ cutting and welding. The central section of the beam pipe remains an integral part of the tracker and is consequently removed with it.

Opening of the inner tracker will be carried out only in a dedicated cooled clean area situated at the surface. To open the detector at one end, the corresponding HF must be removed. This must be done rapidly, with the HF fully cabled, to allow for optimum use of the shut-down period. For this reason, the HF is mounted on a stand supported by a structure composed of three sections, designed to support 400 tons. Mechanical jacks, sunk in the cavern floor, allow movement up or down in a three step operation.

A rotating shielding will provide, on both sides, the interface between the LHC machine and the CMS experiment at the level of the forward calorimeters.

The general planning of the experiment is :

- Surface building (SX5) first phase ready by 1/10/99,
- Reinforcement of conductor on site,
- Winding of the coil on site,
- Activities in SX5,
- Start up of the LHC Machine of 1/07/2005.

Magnetic field

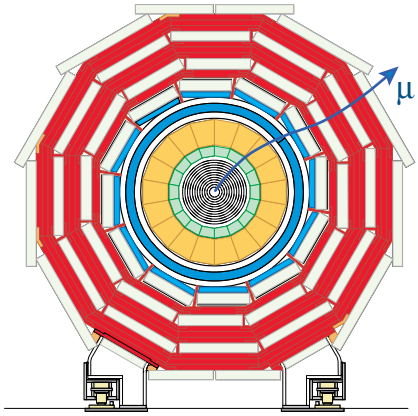

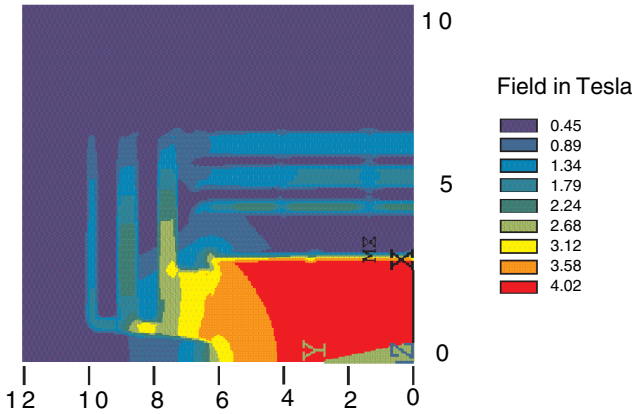

The most important aspect of the overall detector design is the configuration and parameters of the magnetic field. The momentum measurement of charged particles in the detector is based on the bending of their trajectories. High momentum resolution is achievable either through a large bending power or through a very high precision on the spatial resolution and alignment of the detectors. For a similar bending power, the overall size of a solenoidal system is smaller than that of a toroid. The CMS design is thus based on a solenoid providing a very high (4T) magnetic field

Muon measurement and trigger

A solenoid has been chosen for the following reasons:

- With the field parallel to the beam, the bending of the muon track is in the transverse plane, determining the transverse position of the vertex to an accuracy of better than 20 μm. The strong bending in this plane allows triggers based on tracks coming from the vertex.
- The momentum measurement in a solenoid starts at zero radial distance from the beam line.

The CMS design utilizes a superconducting solenoid, 13 m long with a free inner diameter of 5.9 m. The favorable ratio (length/radius) of the solenoid and the high field allow efficient muon detection and measurement up to a pseudo rapidity of 2.4. The inner coil radius is large enough to accommodate the inner tracker and the calorimeters. The magnetic flux is returned via a 1.5 m thick saturated iron yoke instrumented with four stations of muon chambers. The yoke is thick enough to allow safe identification and powerful trigger on muons.

Efficient triggering on muons is a difficult task in hadron colliders. From the outset the CMS philosophy has been to optimize a design which assures a powerful trigger without compromising the performance of other parts of the detector. The goal is to achieve sharp trigger thresholds in order to keep the level-1 trigger rate low — and hence avoid having to implement a hardware level-2 trigger system. As shown in the figure below, a high magnetic field of 4T decreases the level-1 trigger rate by a significant factor. Moreover, the robustness of the CMS muon trigger relies on two independent measurements.

- The first, and more precise one, relies on the measurement of the direction of the muon in the first muon station in the transverse plane. Lowering the field would require a corresponding improvement in the spatial accuracy in the muon chambers.
- The second one uses the measurements in all four muon stations. With a 4T field, the 1.5m of iron in the return yoke is saturated. Lowering the field to 3T would reduce the bending power by 25% and only 1.1 m of iron would be saturated. Four muon stations in a reduced thickness of 1.1 m would not be optimal.

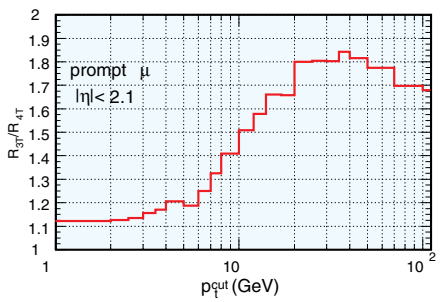

The effect of a different magnetic field strength on the single-muon trigger rate is shown on the left. The plot shows the ratio of the trigger rate with a magnetic field of 3T to the trigger rate with a magnetic field of 4T (CMS design parameter) as function of the transverse momentum of the muon. For high momenta, a 3T field would result in almost a factor two greater trigger rate.

Tracking and calorimetry

In addition to the multilayer muon system, the magnetic field is also coupled with a fully active scintillating crystal electromagnetic calorimeter and a powerful inner tracking system based on fine-grained microstrip and pixel detectors. These features allow a very good measurement of the energies of muons, electrons, other charged particles and photons, typically with a precision of about 1% at 100 GeV. Such a high precision leads to excellent mass resolution for states such as intermediate mass Higgs bosons, new Z' bosons, B mesons in proton-proton collisions or Y states in heavy-ion collisions. Given this detector configuration and precision requirements, a high magnetic field is mandatory for a compact detector based on a single and long solenoid.

Mass Resolution for various states at 4T and 3T.

State	Mass Resolution at 4 T	Mass Resolution at 3 T
H_{SUSY} (300 GeV) $\rightarrow$ ZZ $\rightarrow 4\mu$	2.1 GeV	2.8 GeV
H_{SM} (150 GeV) $\rightarrow$ ZZ* $\rightarrow 4\mu$	0.8 GeV	1.1 GeV
$B^0_d \rightarrow \pi\ \pi$	27 MeV	36 MeV
$\Upsilon \rightarrow \mu\mu$	36 MeV	48 MeV

A field of 4T brings substantial benefits not only to the muon tracking but also for the calorimetry. Maximum benefit from the CMS crystal electromagnetic calorimeter can only be derived if it can be calibrated to an accuracy of a fraction of a percent. This is possible by using copiously produced isolated electrons from the decay of Ws, Zs and b quarks. The energy of the electrons measured in the calorimeters is compared with their momenta measured in the tracker. The number of electrons required is proportional to the square of the standard deviation of the quantity energy/momentum. Optimally both the inner tracking momentum and the electromagnetic calorimeter energy resolutions should be comparable in the relevant range of the energy of the electrons. At present (with a field of 4T) this is indeed the case and the two resolutions are evenly matched.

Changing the magnetic field from 4T to 3T the occupancy in the inner tracker increases by about 40% in the outmost parts of the barrel region and by about 25% in the outer parts of the forward disks. In contrast, it decreases by about 20% in the innermost areas like the silicon barrel detector. For the electromagnetic calorimeter, the trapping of low-momentum charged particles results in a reduced particle flux. As shown in the table below, the flux reduction with increasing field is very significant.

Charged particle energy density/minimum bias event/m^2 in the electromagnetic calorimeter.

Magnetic Field	Mean Transverse Energy Density (GeV/m^2)		
	Barrel		Endcap
	$\|\eta\| = 0$	$\|\eta\| = 1.5$	$\|\eta\| = 2.4$
0 T	0.5	0.55	1.3
2 T	0.3	0.25	0.7
4 T	0.15	0.1	0.4

Magnet system

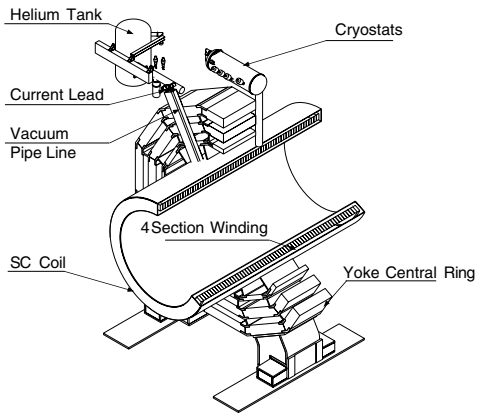

Open view of the superconducting coil inside its vacuum tank

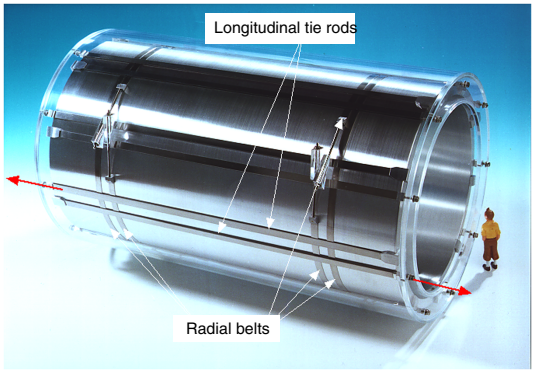

The magnetic yoke contains the muon chambers while the barrel part of the hadron calorimeter, HB, of the electromagnetic calorimeter, EB, and the tracker are situated inside, and supported from the inner shell of the vacuum tank

The CMS magnet system consists of a superconducting coil, the magnet yoke (barrel and endcap), a vacuum tank and ancillaries such as cryogenics, power supplies and process controls. The main parameters are a uniform axial magnetic field of 4 Tesla, a yoke diameter of 14 m across flats, an axial yoke length including endcaps of 21.6 m and a total weight of about 12000 tons. It will be the largest superconducting magnet system in the world: the energy stored into it, if liberated, will be large enough to melt 18 T of gold

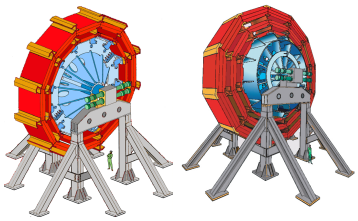

Ferris-Wheel with assembly jig
for central barrel yoke

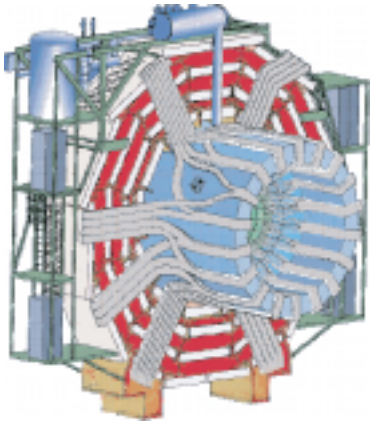

Central barrel yoke, coil, and cables

The magnetic flux generated by the superconducting coil is returned via a 1.5 m thick saturated iron yoke. This yoke is a 12-sided cylindrical structure, divided into endcap and barrel regions. The barrel yoke is divided in 5 rings, is 13.2 m long and has a mass of about 7000 T. Each barrel ring is made up of three iron layers. Connecting brackets join together the steel plates forming the three layers and provide the required structural rigidity. The central barrel ring is the only stationary part around the interaction point and it is used to support the vacuum tank and the superconducting coil. The other four barrel rings and the endcap disks slide on common floor rails, running in the beam direction, to allow insertion and maintenance of the muon stations . Each endcap is built from three independent disks which can be separated to provide access to the forward muon stations. Due to the axial magnetic field the two inner disks must withstand an attraction force of about 85 MN and resist the large bending moments induced. Therefore these two disks are 600 mm thick whereas the outer disk is only 250 mm thick. Each endcap weighs 2300 tons. The vacuum tank is made of stainless steel and houses the superconducting coil. The outer shell of the vacuum tank is attached to the inner part of the central barrel ring and the coil is symmetrically supported from it. All the barrel sub-detectors, HB, EB and tracker are supported by the inner shell of the vacuum tank via a system of horizontal rails.

The superconducting coil system consists of the coil and the ancillary subsystems required for its operation and the protection system. The structure of the superconducting coil is self-supporting , whereby magnetic forces are resisted where they are produced. The reinforced conductor of the four layer CMS coil can sustain by itself all the induced magnetic forces. As the forces induced in the conductor by the magnetic and thermal loads go beyond the yield stress of the pure aluminum a metallurgically bonded mechanical reinforcement is needed. The best way is to have this reinforcement acting axially and tangentially to the coil thus minimizing the conductor construction and winding operation. Ancillaries for the superconducting coil are:

- -the external cryogenic system from the flanges of the outer cryostats,
- -the power supply from the current breakers,
- -the vacuum system from the flange on the pumping line,
- -the process control and the interface to the Slow Control system of the experiment.

The external cryogenic sub-system consists of the compressors, the cold box, the vessels containing the 200 m^3 of pressurized helium gas, the 5000 l LHe container and the cryogenic lines. The cold box and LHe container will be installed near the magnet whereas the compressors and pressure vessel will be at the surface level. The complete system will be installed temporarily on the surface for refrigerator commissioning and coil tests.

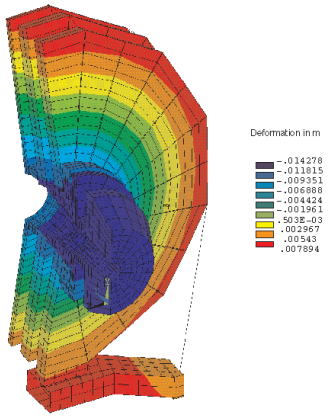

CMS Endcap
Magnetic and gravity loads along the beam direction

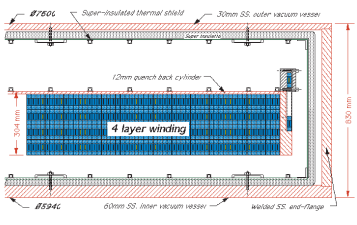

Cross-section through the end of the solenoid

Muon detectors

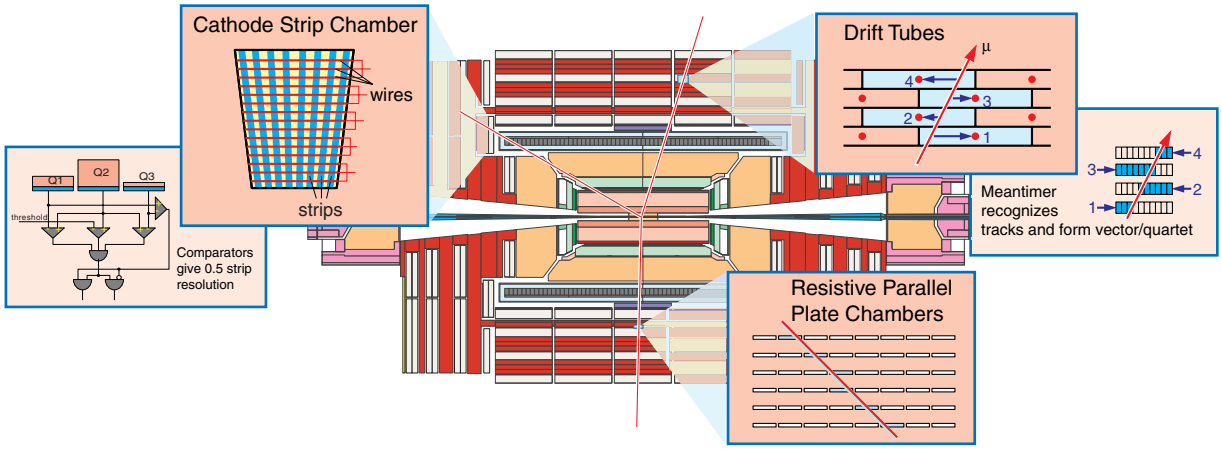

CMS will use three types of gaseous particle detectors for muon identification: Drift Tubes (DT) in the central barrel region, Cathode Strip Chambers (CSC) in the endcap region and Resistive Parallel Plate Chambers (RPC) in both the barrel and endcaps. The DT and CSC detectors are used to obtain a precise measurement of the position and thus the momentum of the muons, whereas the RPC chambers are dedicated to providing fast information for the Level-1 trigger

Drift Tubes

Drift Tubes are used in the Barrel where the Magnetic field is guided and almost fully trapped by the iron plates of the Magnet Yoke. Each tube contains a wire with large pitch (4 cm), and the tubes are arranged in layers. Only the signals from the wires are recorded — resulting in a moderate number of electronic channels needed to read out the detectors. When an ionizing particle passes through the tube, it liberates electrons which move along the field lines to the wire, which is at positive potential. The coordinate on the plane perpendicular to the wire is obtained with high precision from the time taken by the ionization electrons to migrate to the wire. This time (measured with a precision of 1ns), multiplied by the electron drift velocity in the gas, translates to the distance from the wire.

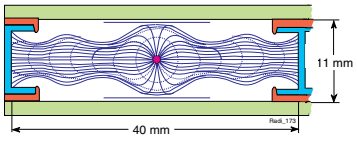

A DT layer is put together gluing to an aluminium plate a set of parallel aluminium I beams. The wires are stretched, held by appropriate end plugs, and the layer is closed by another aluminium plate. Groups of four layers are grown in this way on a precision table. Copper strips are previously glued to the Al plates in front of the wire to better shape the electrostatic field. A full-size final prototype of a DT chamber is shown below. The chamber is 2m x 2.5m in size. The largest DT chambers to be used in CMS will have dimensions of 4m x 2.5m in size.

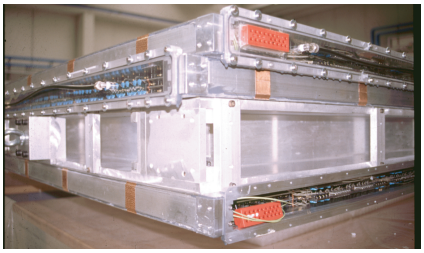

Cathode Strip Chambers

Cathode Strip Chambers are used in the Endcap regions where the magnetic field is very intense (up to several Tesla) and very inhomogeneous. CSCs are multiwire proportional chambers in which one cathode plane is segmented intro strips running across wires. An avalanche developed on a wire induces a charge on several strips of the cathode plane. In a CSC plane two coordinates per plane are made available by the simultaneous and independent detection of the signal induced by the same track on the wires and on the strips. The wires give the radial coordinate whereas the strips measure ϕ.
In addition to providing precise space and time information, the closely spaced wires make the CSC a fast detector suitable for triggering. CSC modules containing six layers provide both a robust pattern recognition for rejection of non-muon backgrounds and also efficient matching of external muon tracks to internal track segments.

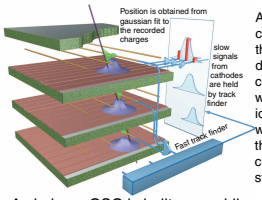

Artist scheme of a CSC chamber, with a sketch of the mechanism of signal detection. The electrons are collected by the wire, whereas a cloud of positive ions moving away from the wire of the wire and toward the cathode induces a current on the cathode strips perpendicular to the

A six-layer CSC is built assembling together 7 Honeycomb panels. Three of them support two wire planes each, one on each face of the plate, wired at the same time as shown in the photograph below. The other four plates have the etched strip. The two inner plates have strips on both faces, whereas the two outer plates (closing the chamber) have strips on only one face.

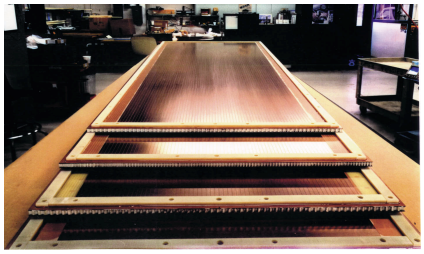

Resistive Parallel plate Chambers

Resistive Parallel plate Chambers are fast gaseous detectors whose information is at the base of the triggering process. RPCs combine a good spatial re-solution with a time resolution of 1 ns, comparable to that of scintillators. The RPC is a parallel plate counter with the two electrodes made of very high resistivity plastic material. This allows the construction and operation of very large and thin detectors that can operate at a high rate and with a high gas gain without Resistive Parallel plate Chambers are fast gaseous detectors whose information is at the base of the triggering process. RPCs combine a good spatial re-solution with a time resolution of 1 ns, comparable to that of scintillators. The RPC is a parallel plate counter with the two electrodes made of very high resistivity plastic material. This allows the construction and operation of very large and thin detectors that can operate at a high rate and with a high gas gain without developing streamers or catastrophic sparks. The high gain and thin gap result in a small but very precise delay for the time of passage of an ionizing particle. The high resistivity electrode

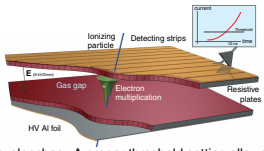

The electric field inside a RPC is uniform. Electrons made free by the ionizing particle near the cathode generate a larger number of secondary electrons (exponential multiplication). The detected signal is the cumulative effect of all the avalanches. A proper threshold setting allows the detection of a signal dominated by the electrons generated near the cathode. The threshold setting determines to a large extent the time delay of the pulse, the time resolution and also the efficiency. With a proper choice of the resistivity and plate thickness, the rate capability can reach several thousand Hertz per cm^2.
The drawing shows the simplicity of an RPC detector: one of the two resistive plates holds a glued array of small 2mm thick spacers having a typical pitch of 10 cm. Also glued on the plate is the border that will guarantee the chamber tightness. The second plate is then placed on top and the detector is completed.

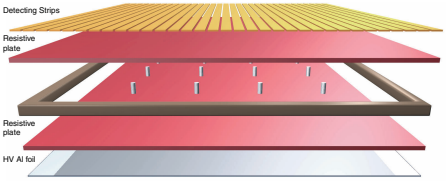

Muon system

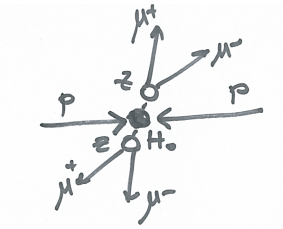

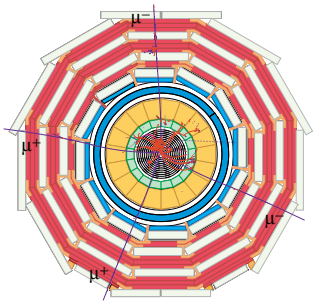

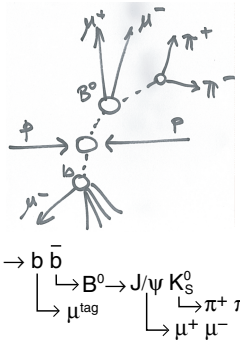

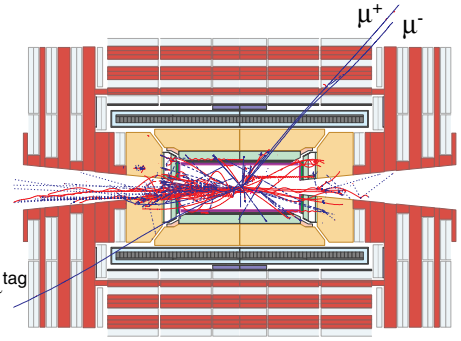

Muons are expected to provide clean signatures for a wide range of physics processes. The task of the muon system is to identify muons and provide, in association with the tracker, a precise measurement of their momentum. In addition, the system provides fast information for triggering purposes — a challenging problem at the LHC.

The muon detectors, placed behind the calorimeters and the coil, consist of four muon stations interleaved with the iron return yoke plates. They are arranged in concentric cylinders around the beam line in the barrel region, and in disks perpendicular to the beam line in the endcaps

Muon identification

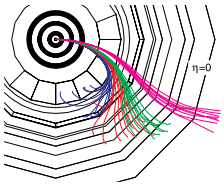

p_t = 3.5, 4.0, 4.5, 6.0 GeV

Muon identification is ensured by the large thickness of the absorber material (iron) which cannot be traversed by particles other than neutrinos and muons.
There are at least 10 interaction lengths (λ) of calorimeters before the first station and an additional 10 λ of iron yoke before the last station. The identification is achieved by lining up the hits in at least two out of the four muon stations. The presence of multiple stations also enables the control of hadronic shower punchthrough and hard muon bremsstrahlung.

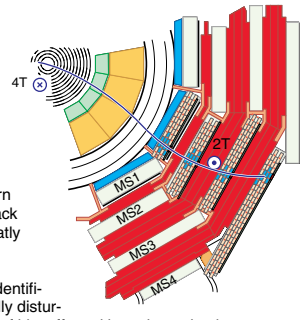

With multiple chamber layers in each station providing many distributed measurement points, the pattern recognition of track segments is greatly simplified.

Track segment identification is minimally disturbed by rejection of hits affected by noise or background such as soft δ-rays and electrons from neutrons and gammas. The thickness of the absorber between the stations (30 to 75 cm) also prevents station-to-station correlations due to high energy muon radiation.

Momentum measurement

The momentum measurement utilises the bending of charged tracks in the magnetic field produced by the coil and conducted by the return yoke. The solenoidal field of CMS bends tracks in the (r,ϕ) plane perpendicular to the beam axis. The muon transverse momentum, p_t, may be determined in three ways:

- bending angle measurement immediately after the coil,
- sagitta measurement in the return yoke.
- measurement of the sagitta of the track in the inner tracker

The first two measurements are performed by the muon detectors alone, independently of the inner tracker for a "stand alone" measurement and can be used both by the trigger and the off-line reconstruction program. The reconstruction procedure is naturally robust against backgrounds because of the redundancy of the measurements. The best off-line resolution is obtained when all three methods are combined with the vertex constraint of 15 μm.

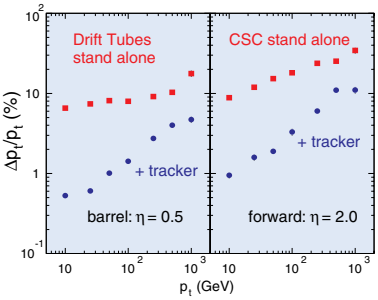

The resolution at low p_t is limited by multiple Coulomb scattering; the resolution at high p_t is limited by the chamber resolution. The strong bending due to the high field is a great benefit in both cases. With resolutions of the order of 100 μm per station, the standalone measurement is dominated by multiple Coulomb scattering for p_t below 200 GeV. With the full measurement, including the tracker, the muon sign can be recognised in the entire kinematical range ($p < 7$ TeV, $|\eta| < 2.4$).

Triggering on muons

A fundamental aspect of the CMS muon system design is that it allows for the identification of muons and the estimate of their transverse momentum online, for triggering purposes. The muon trigger system has to perform these tasks with high efficiency and precision in order to reduce the proton-proton interaction rate of ~ 1GHz to a few kHz by demanding that the transverse momentum of the muons seen exceeds a certain threshold.

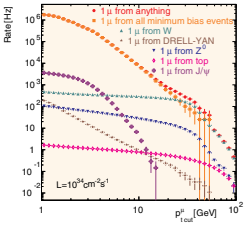

The need for a fast determination of the muon momentum also guided the choice of the CMS magnet which bends muon trajectories in the transverse plane. A few trigger planes with modest azimuthal segmentation can then be used to measure the muon direction after the solenoid and apply a cut on the muon transverse momentum, p_t. The figure on the left shows the rate with which muons are produced from various physics processes.

Another basic requirement of the muon trigger system is to reject efficiently many different types of background hits that can simulate genuine, high-p_t prompt muons. These backgrounds arise from hadronic punchthroughs, debris from muon interactions with matter, thermal neutrons, beam halo in the forward direction and finally noise in the electronics. A key feature of the design is to combine information from different muon detectors: Resistive Plate Chambers (RPC) and Drift Tubes (DT) in the barrel and RPCs and Cathode Strip Chambers (CSC) in the endcaps. These detectors have different responses to the various backgrounds. As an example, RPCs provide a very accurate time measurement, whereas DTs provide an accurate position measurement. The efficiencies for triggering on real muons are complementary

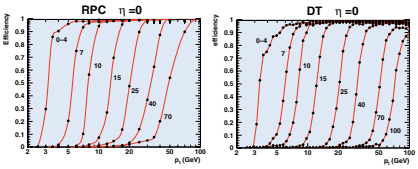

New physics

Supersymmetry (SUSY) postulates a deeper relationship between matter particles (spin-1/2 or "fermions") and force carriers (integer spin or "bosons") than the Standard Model (SM). In SUSY, each fermion has a "superpartner" of spin-0 while each boson has a spin-1/2 superpartner. The Higgs sector is also extended to at least five Higgs bosons in the Minimal Supersymmetric Standard Model (MSSM). To this day, no superpartners have been observed: SUSY must be a broken symmetry, i.e. the superpartners must have masses different than those of their partner particles.

Despite the doubling of the spectrum of particles, SUSY has many merits: it is elegant; assuming the existence of superpartners with TeV-scale masses, the Strong, Weak and Electromagnetic force strengths become equal at the same energy of ~ 10^{16} GeV (the "GUT scale"); it also provides a natural explanation of why the Higgs mass can be low ($\lesssim$ 1 TeV). In SUSY theories, there is even room for explaining the dark matter in the Universe as being due to "neutralinos". If SUSY is a true symmetry of Nature and it is realized at the TeV scale, it will almost certainly be seen in CMS

SUSY Higgs bosons

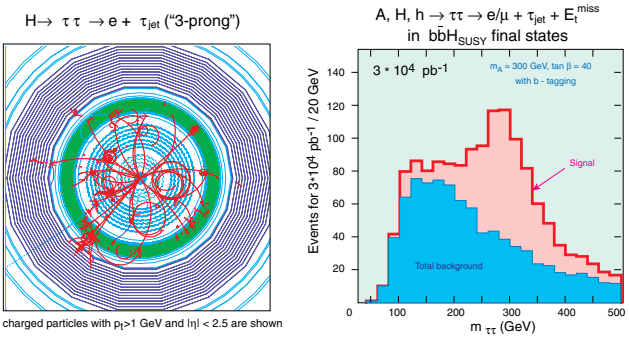

In the MSSM there are 5 Higgs bosons: h^0, H^0, A^0 and $H^\pm$ decaying through a variety of decay modes to γ, $e^\pm$, $\mu^\pm$, $\tau^\pm$ and jets in final states. Above left: an example of a SUSY Higgs decay in CMS. On the right is the reconstructed $\tau\,\tau$ mass spectrum

Sparticle discovery ranges

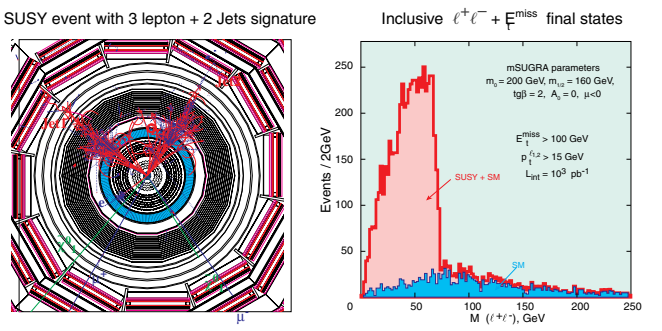

Production of sparticles may reveal itself though some spectacular kinematical spectra, with a pronounced "edge" in the $\ell^+\ell^-$ mass spectrum reflecting $\tilde{\chi}_2^0 \to \ell^+\ell^-\tilde{\chi}_1^0$ production and decay. An example of such an edge in the inclusive di-lepton mass spectrum and of an event with tri-lepton are shown above

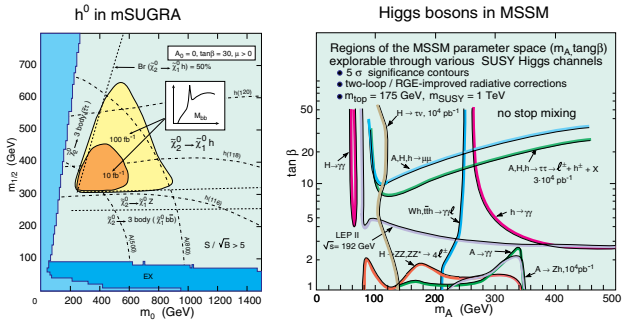

Example of the domain of parameter space of mSUGRA-MSSM where the $h^0 \to b\bar{b}$ can be observed

The search for the various MSSM Higgs bosons in different decay modes allows the exploration of most of the parameter region (tanβ,m_A)

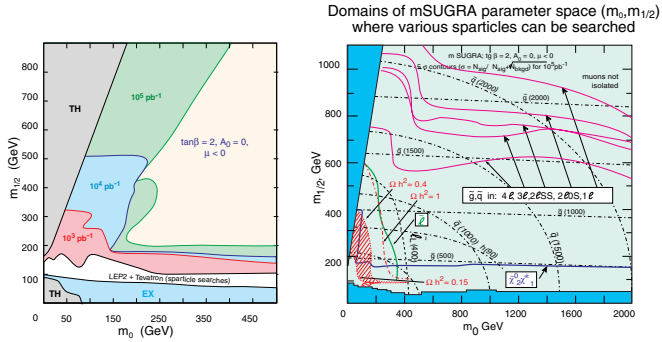

Domain of mSUGRA parameter space where the "edge" in $\ell^+\ell^-$ mass, in inclusive isolated two - leptons + E_t^{miss} final states, should be visible at various luminosities

Gluinos and squarks can be looked for in various channels with leptons + E_t^{miss} + jets and discovered for masses up to ~ 2.2 TeV. Sleptons can be discovered for masses up to ~ 350 GeV. The region of parameter space $0.15 \lesssim \Omega\, h^2 \lesssim 0.4$ — where $\tilde{\chi}_1^0$ would be the Cold Dark Matter particle — is contained well within the explorable region

Tracker electronics

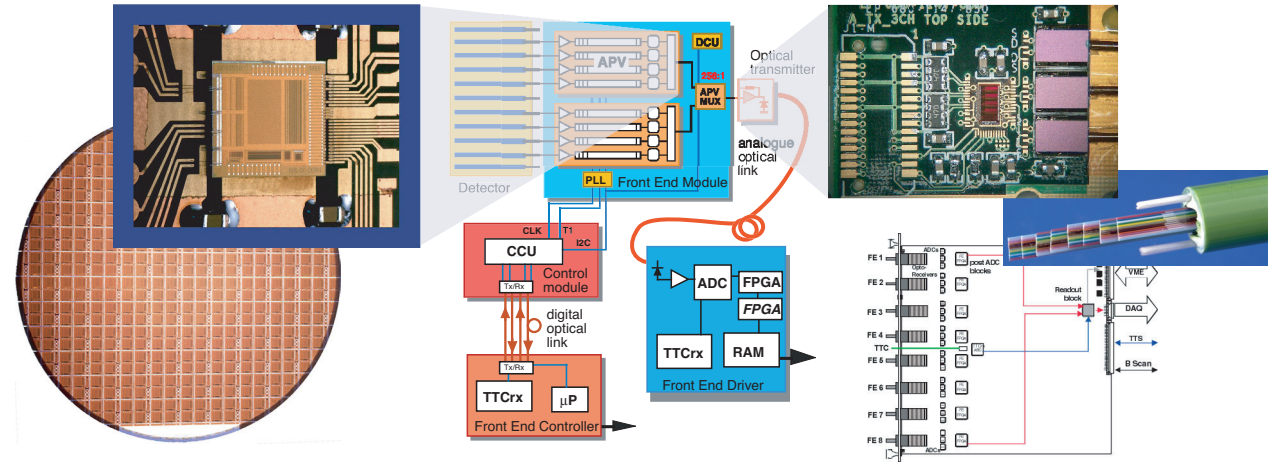

The system will provide analogue data from ~10 million channels of the microstrip tracker with minimal power and material. Electronic noise should be sufficiently low to ensure high efficiency and bunch crossing identification. Performance is ultimately limited by the speed and magnitude of detector signals and the radiation environment. Lifetime doses of 100kGy (10Mrad) and fluences of 2 x 10^{14} hadrons cm^{-2} are expected in the innermost layers

The target is an equivalent noise charge below 2000 electrons over the detector lifetime for front-end power consumption ~2mW/channel. Analogue data are preferred for good position resolution, from charge sharing between strips, and robustness, as common mode noise may be a challenge. The system minimises custom radiation hard electronics inside the tracker. Zero suppression of data outside the tracker allows possible upgrades through technology and cost evolution of commercial components

APV Front End circuit

Each microstrip is read out by a charge sensitive amplifier whose output voltage is sampled at the LHC 40MHz rate. Samples are stored in an analogue pipeline for up to 4μs and, following a trigger, are processed by an analogue circuit using a weighted sum algorithm to measure signal amplitude and associate the bunch crossing with the hit. Pulse height data are multiplexed from pairs of front-end chips, sending differential signals over a short twisted pair cable to a laser where electrical signals are converted to infra-red pulses and transmitted over a 100m fibre optic cable to the counting room adjacent to the cavern

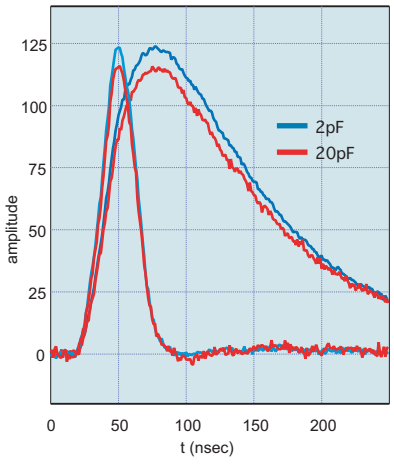

Optical link

The optical link employs edge-emitting semiconductor laser transmitters operating at the telecommunications wavelength of 1310 nm. The lasers are assembled with single mode fibre pigtails in a low mass package developed in collaboration with industry. All link components have been shown to be extremely radiation hard. A minimum current is required before laser action starts. Above threshold the light output power is extremely linear with drive current. After irradiation, an increase in threshold current is observed but the laser characteristic remains linear

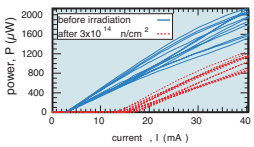

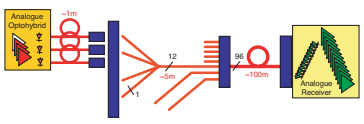

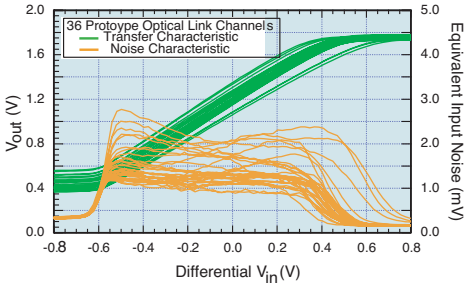

Front End Driver

Pulse height data are received by a photodiode-amplifier on the Front End Driver which digitises and processes the signals, including reordering and pedestal subtraction, and stores results in a local memory for the higher level data acquisition. In high luminosity conditions when CMS is operating at the maximum trigger rate, cluster finding will be carried out on the FED to reduce the data volume

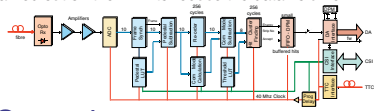

Control system

The Front End Controller supervises control and monitoring of the front-end electronics and is the interface to the CMS Timing Trigger and Command system. Digital optical links, using the analogue link components, transmit triggers, clocks and control data. Internally, digital transitions are recovered by photodiode-amplifiers and distributed electrically by a Communication and Control Unit (CCU) to detector modules. Clocks are recovered by Phase Locked Loop (PLL) chips on each module for high reliability and minimum phase jitter. CCU modules can be configured as rings to match the tracker topology and reduce cost

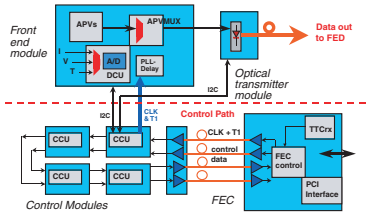

Tracking system

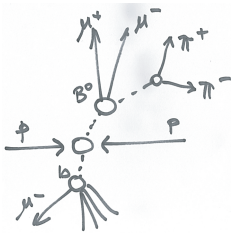

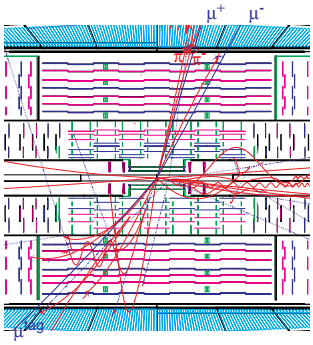

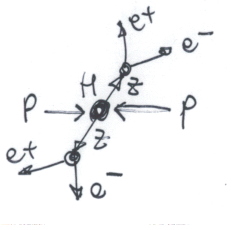

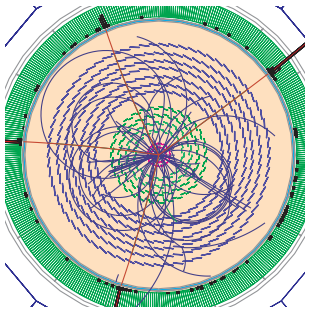

A robust and versatile tracking system is of the utmost importance for an experiment designed to address the full range of physics which can plausibly be accessed at the LHC. The CMS tracking system is designed to reconstruct high-p_T muons, isolated electrons and hadrons with high momentum resolution and an efficiency better than 98% in the range $|\eta|<2.5$. It is also designed to allow the identification of tracks coming from detached vertices. Such vertices arise from decays of b quarks, which provide very useful signatures for a broad spectrum of new physics

Track identification

The LHC environment (with its high radiation levels shown below), the varied nature of the interesting physics signatures, and the constraints of compatibility with the excellent electromagnetic calorimetry of CMS, present formidable challenges which a successful tracking system must overcome.

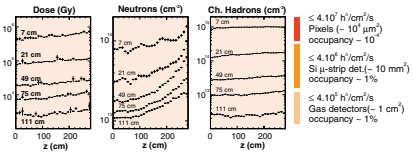

The strategy adopted to address these challenges is to provide a set of coordinate measurements of sufficient precision and robustness such that track reconstruction can be reliably performed based on a relatively small number of measurements per track. In addition, the tracking system is embedded in a 4T magnetic field which forces low-p_T particles into small-radius helical tracks, resulting in reduced occupancy at larger radii.

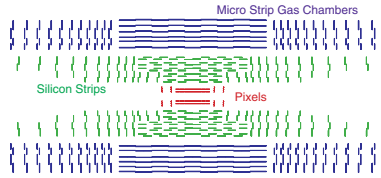

Three detector technologies are employed, each best matched to satisfying the stringent resolution, granularity and robustness requirements in the high, medium and low occupancy regions. These are Pixels, Silicon Microstrip and Micro Strip Gas Chambers (MSGC) respectively.

To achieve reliable track identification, the detector segmentation is such that typical channel occupancies are kept at about the 1% level everywhere in the tracker.

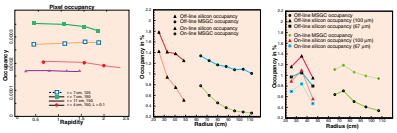

Momentum measurement

The momentum of electrically charged particles is determined from the bending of the track trajectory in the magnetic field of CMS.

The trajectory of a charged particle inside a magnetic field of strength (in Tesla), perpendicular to its velocity, v, is a circle of radius R (in meters). Reconstructing this trajectory yields R. The particle's momentum transverse to the B field, p_T, measured in GeV/c, is then given by $p_T = 0.3\ B\ R$

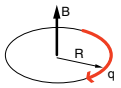

High transverse momentum (p_T) isolated tracks are reconstructed with a transverse momentum resolution of better than $\delta p_T/p_T \approx (15 p_T \otimes 0.5)\%$, with p_T in TeV, in the central region $|\eta| \le 1.6$, gradually degrading to $\delta p_T/p_T \approx (60 p_T \otimes 0.5)\%$ as $|\eta|$ approaches 2.5.

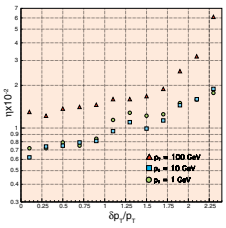

Combining the tracking system with the outer muon chamber system, the resolution of the measurement of the momentum of muons above about 100 GeV is given by $\delta p/p \approx (4.5 p^{1/2})\%$, with p in TeV, even for pseudorapidities extending to at least $|\eta|=2$. This results in a momentum resolution better than 10% even at a momentum of 4 TeV.

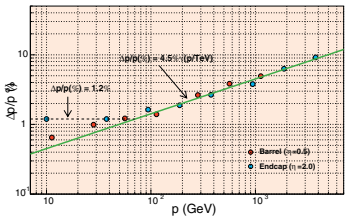

Track reconstruction is especially challenging in a dense jet environment. The fine granularity of the CMS tracking system results in a high efficiency of reconstruction (95%) for charged hadrons with p_T above 10 GeV. The reconstruction efficiency for muons is better than 98% over the full pseudorapidity range. High energy electrons are reconstructed with an efficiency above 90%.

Vertex identification

The ability to reconstruct the decay vertices of long-lived particles is crucial for numerous physics analyses. The position of such vertices in the tracking volume depends on the lifetime of the decaying particle. Long-lived particles (e.g. K_s mesons) travel several cm before decaying. B mesons decay more rapidly (they decay within 1-2 mm) but their decay point is still discernible thanks to the excellent resolution of the impact parameter measurement.

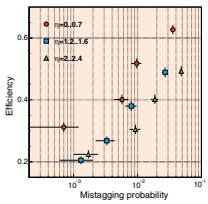

A vertex displaced from the primary proton-proton collision point also arises from decays of hadrons containing a b quark. The reconstruction of such vertices is crucial for "b-tagging", i.e. in the identification of a jet as arising from a b quark. b-tagging is a very important tool for many physics studies, from the search of low-mass Higgs bosons to studies of the top quark (which always decays to a b quark). The figure displays the efficiency for tagging b-jets with E_T=100 GeV as a function of the probability of misidentifying jets originating fromlight quarks or gluons.

K_s identification is very important for the reconstruction of the decay $B^0 \to J/\psi K_s$ which will be used to study CP violation in the B system. As shown in the figure on the right, the average efficiency of reconstrucing K_s's from B meson decays is typically 50% when the K_s decays inside the barrel tracking volume (and =33% when it decays in the forward tracking volume).

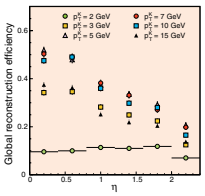

The high efficiency for reconstructing secondary vertices, is supplemented by the very high resolution of the reconstrution of both the invariant mass of the decaying particle and its proper decay time.

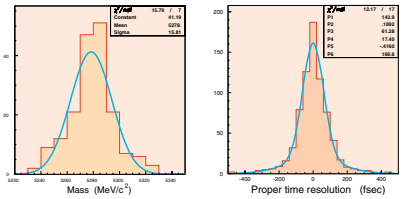

Trigger and data acquisition

Data Acquisition Main Parameters		
Collision rate		40 MHz
Level-1 Maximum trigger rate		100 kHz
Average event size	=	1 Mbyte
No. of electronics boards	=	10000
No. of readout crates	=	250
No. of In-Out units (200-5000 byte/event)	=	1000
Event builder (1000 port switch) bandwidth		1 Terabit/s
Event filter computing power	=	5 10^7 MIPS
Data production	=	Tbyte/day

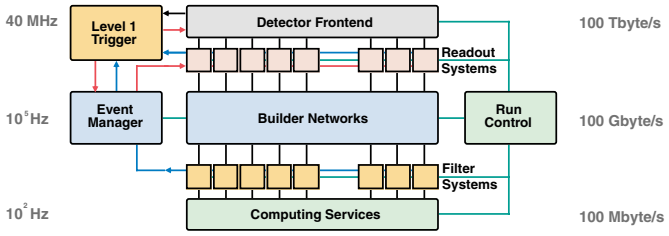

Trigger and Data Acquisition baseline structure

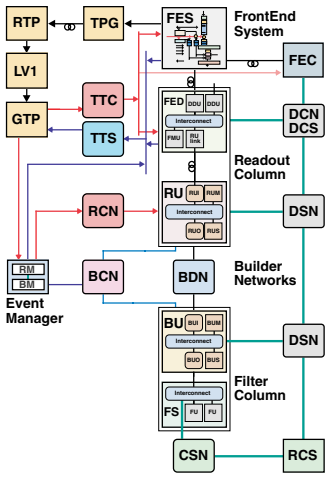

FLT	**FIRST LEVEL TRIGGER**
TPG	Trigger Primitive Generator
TDL	Trigger Data Link
RTP	Regional Trigger Processor
LV1	Calo & μ Trigger Processors
GTP	Global Trigger Processor
TTC	Timing, Trigger & Control
TTS	Trigger & Throttle System
EVB	**EVENT BUILDER**
BN	Builder Networks
BDN	Builder Data Network
RCN	Readout Control Network
BCN	Builder Control Network
EVM	Event Manager
RM	Readout Manager
BM	Builder Manager
FES	Front End System
DDL	Detector Data Link
RC	Readout Column
FED	FrontEnd Driver
FMU	Fast Monitoring Unit
DDU	Detector Dependent Unit
RDL	Readout Data Link
RU	Readout Unit
RUI	Readout Unit Input
RUM	Readout Unit Memory
RUO	Readout Unit Output
RUS	Readout Unit Supervisor
FC	Filter Column
BU	Builder Unit
BUI	Builder Unit Input
BUM	Builder Unit Memory
BUO	Builder Unit Output
BUS	Builder Unit Supervisor
FS	Filter Subfarm
FU	Filter Unit
HLT	High Level Trigger
RCS	**RUN CONTROL SYSTEM**
DCN	DAQ operation control and monitor
DDB	DAQ data bases
DCS	Detector Control System
DCN	Detector Control Network
FEC	FrontEnd Control
CDL	Control Data Link
CS	**COMPUTING SERVICES**
CSN	Computing and Services Network
DSN	DAQ Services Network
DA	Data archives

Computing and Communication main subsystems

At the LHC, the proton beams cross each other 40,000,000 times each second. At the highest LHC beam intensities, there will be roughly 25 proton-proton collisions for each crossing. Recording all the information from these collisions in the CMS experiment, requires, for every second of operation, the equivalent of 10,000 Encyclopaedia Britannica

The task of the Trigger and Data Acquisition System is to select, out of these millions of events, the most interesting 100 or so per second, and then store them for further analysis. An event has to pass two independent sets of tests, or Trigger Levels, in order to pass the TriDAS examination. The tests range from simple and of short duration (Level-1) to sophisticated ones requiring significantly more time to run (High Levels 2, 3, ...)

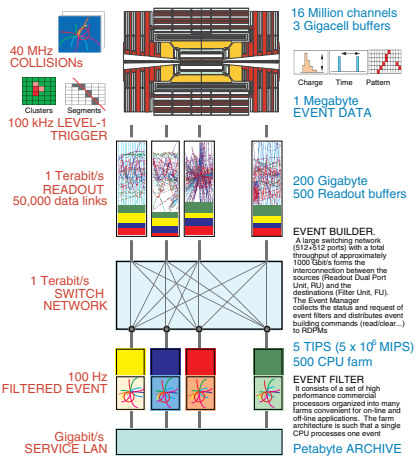

At Level-1 (LV1), the selection is carried out by special hardware processors seeking simple signs of an interesting event, e.g. a group of calorimeter cells with a lot of energy in them or muon chamber hits lying on given paths. The LV1 Trigger is very fast: it runs for less than one millionth of a second and selects the best 100,000 events each second. After Level-1 accepts an event, the data for that event is stored in 500 independent memories (RDPMs), each one connected to a different part of the CMS detector

The next test, "Level-2" uses information from more than one piece of the detector. The next step is therefore to assemble the data corresponding to the various pieces of the CMS detector in a single location, a task referred to as "event building". In CMS, there will be a large switch that will connect all 500 RDPMs to a farm of computers. The latter are ready to accept data and run the Level-2 and Level-3 tests

Level-2, running on commercial processors, has more time and information to make a decision: it can take roughly thousandths of a second to decide, and the detector information available is more detailed

Finally, at Level-3, the full event has been assembled, and one can run very sophisticated physics algorithms looking for complex signatures. This is where particle tracks are matched to hits in the muon chambers, and where a photon is identified as a cell with high electromagnetic energy and no track pointing to it! Throughout this process, the DAQ system monitors the CMS detector and corrects for any malfunction

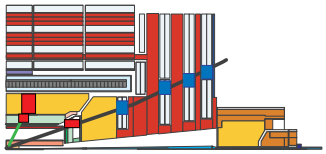

Level-1 trigger. 40 MHz input :
- Specialized processors (25 ns pipelined, latency < 1μs
- Local pattern recognition and energy evaluation on prompt macro-granular information from calorimeter and muon detectors
- Particle identification: high p_t electron, photon, muon, jets, missing E,

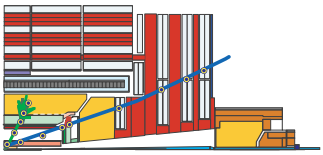

High trigger levels (>1). 100 kHz input :
- Large network of processor farms
- Clean particle signature. All detector data
- Finer granularity precise measurement
- Effective mass cuts and event topology
- Track reconstruction and detector matching
- Event reconstruction and analysis

Tracking detectors

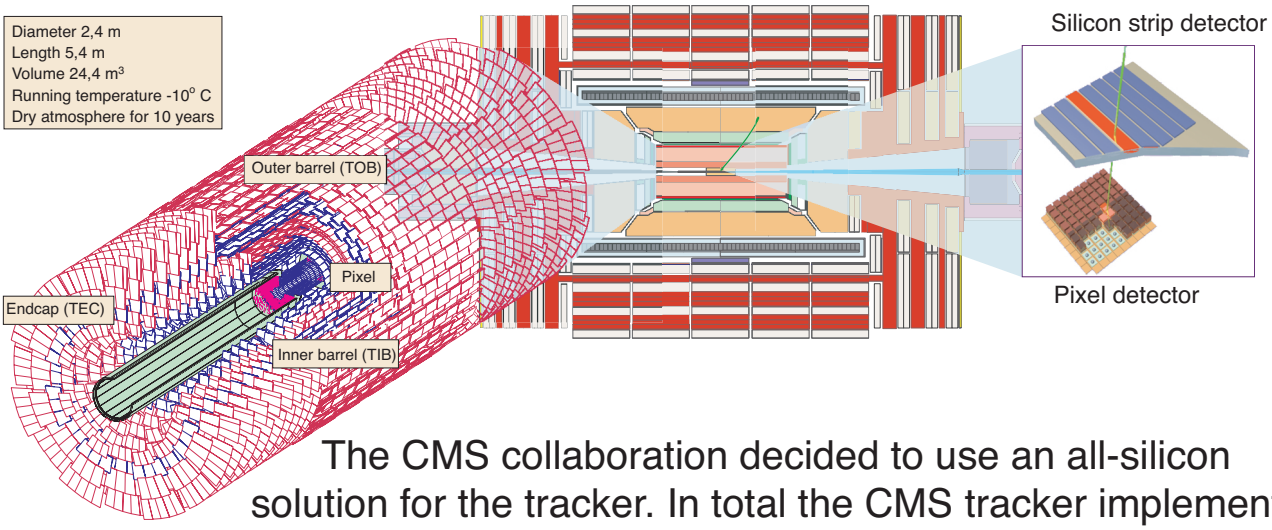

The CMS collaboration decided to use an all-silicon solution for the tracker. In total the CMS tracker implements 25000 silicon strip sensors covering an area of 210 m^2. Connected to 75000 APV chips, one has to control 9600000 electronic readout channels, needing about 26 million microbonds. This large detector system will be realized, applying industrialized methods in production and quality assurance.

Pixel Detectors

At the smallest radii from the beam line (at 4 and 7 cm at low luminosity and at 7 and 11 cm at high luminosity) the interaction region is surrounded by two barrel layers of Silicon Pixel detectors. Two endcap disks cover radii from 6cm to 15cm.

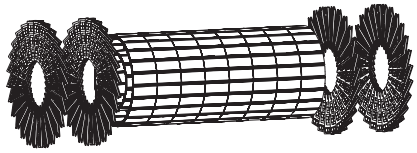

The pixel layers are composed of modular detector units. Each module consists of a thin, segmented sensor plate with highly integrated readout chips connected to them using the bump bonding technique, as shown below.

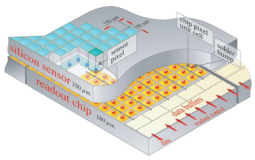

Schematic view of a pixel detector element. Each sensor pixel is connected via a solder bump to a pixel unit on the readout chip, where the signal is amplified. The hit data are stored on the edge of the chip where they wait for the trigger information.

The cell size in the Pixel detectors is 150x150 μm^2. The pixels used are n-on-n devices so that, in the barrel, their response is strongly affected by the 34° Lorentz angle of the drift of electrons. The barrel Pixel geometry is deliberately arranged so that this large Lorentz angle induces significant sharing of charge across neighboring cells and this results in spatial resolutions of ≈ 10 and 15 μm in the ϕ and z coordinates respectively.

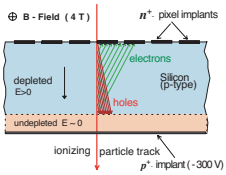

Charge sharing induced by the Lorentz drift. The sensor material is silicon in which the electron drift angle is three times larger than for holes. Therefore, n-type pixels, which collect electrons, will be used. When the electrons arrive at the pixel surface, they are spread over an rϕ distance of ≈ (detector thickness) x tan(34°).

Silicon Strip Detectors

The layout for the silicon strip detector has four inner barrel (TIB) layers assembled in shells, layers 1&2 are double sided , complemented by two inner endcaps (TID) each composed of three small discs. The outer barrel (TOB) structure, where the modules are assembled in six concentric layers (layers 1&2 double sided), closes the tracker towards the calorimeter.

Two endcaps (TEC) ensure a pseudorapidity coverage of η = 2.5. The endcap modules are mounted in 7 rings on 2x9 discs consisting of wedge shaped petals, each covering 1/16 of 2 π. The detectors of ring 1,2,5 are made of double sided modules. Each one is composed out of two single sided sensors mounted back to back, one tilted by an angle of 100 mrad with respect to the other sensor giving the phi coordinate.

Silicon sensors are highly suited for high occupancy and high resolution experiments, due to their fast response and small pitches, ranging from 80 to 205 μm. In the outer regions, higher noise due to "long" strips is compensated by larger signal height using 500 μm thick sensors instead of 300 μm. 6 inch wafer technology made this huge construction at a reasonable prize and effort possible.

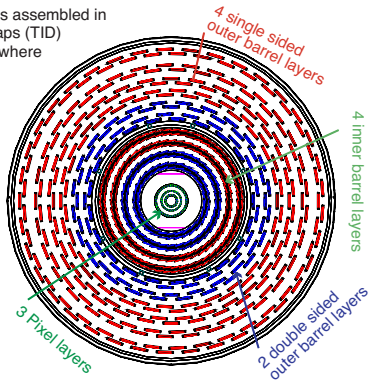

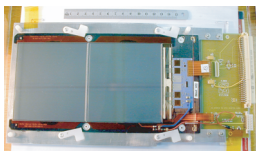

First assembled TOB module

A detector module is the basic functional sub-unit of the silicon tracking system. Each module consists of three elements: a set of single sided sensors, a mechanical support structure and the readout hybrid.

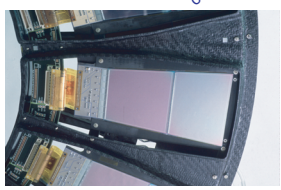

TEC wedge shape module

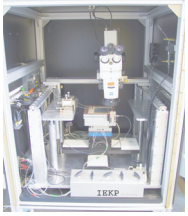

Fully automatic probe station

Quality assurance, assembly and bonding will be realized under quasi industrial conditions with high multiplicity : 4 centers are surveilling the overall sensor quality using fully automatic probe stations, 3 centers are monitoring the process quality and finally 2 centers are checking the radiation hardness. Assembly robots in 7 centers plus industrial bonding machines in 12 places ensure high quality and reliability over the long construction period. All parameters and logistics are monitored using a special global database.

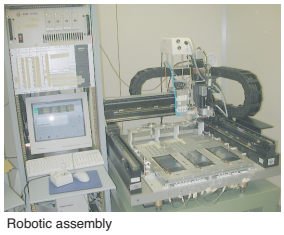

Robotic assembly

How to survive 10 years in the harsh LHC environment!
- To compensate interstrip capacitance increase, resulting in higher noise, CMS uses silicon with <100> crystal orientation, which is less affected by irradiation.
- Low resistivity silicon in the inner region starts with a higher depletion voltage but ending with lower depletion voltage after type inversion and 10 years of LHC operation. New strip layout optimizes the field configuration, avoiding strip breakdown at high voltage.